Dynamics and Control of a Single Wheel, Gyroscopically Stabilized Robot

by
Kwok-wai Au

A Thesis Submitted in Partial Fulfillment
of the Requirements for the Degree of
Master of Philosophy
in
Mechanical and Automation Engineering

August 30, 1999


香港中文大學
圖書館系統
21 FEB 2000
UNIVERSITY
LIBRARY SYSTEM
THE UNIVERSITY OF HONG KONG

摘要

單輪陀螺平衡機器人，我們稱之為“Gyrover”，是一種新型的移動機器人。它可以實現機器人快速運動下的動態平衡。一般來說，這種機器人是一個滾動輪，通過旋轉的飛輪來控制其轉向，並且用驅動馬達來推動它前進。旋轉飛輪的功能相當于陀螺，可以保持機器人的平衡，並且通過調節它的傾斜角度可以控制機器人的轉向。上述的結構特點使得這種單輪機器人比多輪式靜態平衡移動機具備許多優點，包括良好的動態穩定性，抗姿態干擾性，靈活性，低滾動阻力，跌倒恢復能力，以及水陸兩用的功能。然而與此同時，這種新型的機器人也帶來了一些建模和控制上的挑戰性的問題。首先，在單輪和飛輪之間存在高度的耦合性。其次，這個系統由于存在滾動約束以及在滾動方向上無驅動而受到兩種非完整約束。第三，這種機器人在本質上存在側向的不平衡性。因此，本篇論文的目的就是要研究這種機器人上述的基本特性，從而開發出單輪陀螺平衡機器人的自主控制系統。

為了研究這個動態平衡但靜態不平衡的系統，我們首先推導出機器人的動力學模型，其中包括運動學約束和運動方程。在推導過程中，我們把機器人看作是三種元件的組合體，也就是由兩杆機械臂聯接的滾動輪，內部機構和飛輪。在動力學方程中我們通過對飛輪傾斜角度這個變量進行解耦來簡化該模型。我們證明了這是一個非完整，部份無驅動以及非最小系統。在本文中，我們揭示了這種動態耦合的本質，包括機器人的穩定性和飛輪傾角對機器人轉向的影響，並且通過一些基本實驗驗證了這一模型。

由於這種單輪機器人存在側向不穩定性，因此想要控制它首先就要使

系統平衡。但是因為在側向上沒有驅動器來維持機器人的平衡，我們只能利用飛輪與滾論之間的耦合，通過間接控制飛輪的傾角來控制機器人的傾角。在本文中，我們提出一種線性反饋控制方法，通過調節飛輪傾角使機器人能在任何傾角處達到平衡。

自主式移動機的一項基本功能就是能夠跟蹤預定的路徑。為此我們設計了一種直線跟蹤控制器，它可以讓機器人從初始位置起跟蹤任何目標直線。這種控制器的基本思想來源于單車的運動。由于存在滾動約束，單輪機器人只能跟蹤曲率連續的路徑，因此，我們首先通過控制路徑的曲率來設計機器人跟蹤目標直線的前進速度和轉向速度。另外，因為這種機器人上沒有安裝類似單車前輪的轉向裝置，所以我們設計的控制器採用了顯性反饋的方法使機器人可以平衡在預定的傾角上，從而使機器人的轉向速度趨進理想的轉向速度。這種直線跟蹤控制器避免了直接解決受兩種非完整約束的復查的機器人模型。而且，該方法還可以用于跟蹤任何預定的圓弧軌跡。

Abstract

The single wheel, gyroscopically stabilized robot, called Gyrover, is a novel concept of mobile robots which provides dynamic stability for rapid locomotion. Generally, it is a sharp-edged wheel actuated by a spinning flywheel for steering and a drive motor for propulsion. The spinning flywheel acts as a gyroscope to stabilize the robot and it can be tilted to achieve steering. This configuration conveys significant advantages over multi-wheel, statically stable vehicles, including good dynamic stability and insensitivity to attitude disturbances; high maneuverability; low rolling resistance; ability to recover from falls; and amphibious capability. At the same time, the robot concept also brings a number of challenging issues in modeling and control. First, it is a highly coupled dynamic system between the wheel and the flywheel. Second, it is subject to two nonholonomic constraints due to the rolling constraints and underactuation in the roll direction. Third, it is inherently unstable in the lateral direction. In this thesis, the goal is to study this fundamental characteristics which will lead to development of the autonomous control of Gyrover.

In order to study such a dynamically stable but statically unstable system, we develop dynamic model of the robot, including kinematic constraints and motion equations. In deriving the model, we consider the robot as a combination of three components which are a rolling disk, an internal mechanism and a flywheel, and are linked by a two-link manipulator. We simplify the model by decoupling the tilt angle of the flywheel from the dynamics. It is shown that the model of the robot is nonholonomic, underactuated and non-minimum phase. We reveal the nature of the dynamic coupling and robot dynamic properties such as the stabilization and tilting effect of the flywheel to the robot. Preliminary experimental results have verified the developed model.

Owing to the lateral instability of the robot, the first step in controlling the robot is to stabilizing the system. Because no actuator can be used for stabilization in the lateral direction, the lean angle of the robot can be controlled only indirectly through tilting the flywheel due to the coupling effect between the two. We propose a linear state feedback to stabilize the

robot to any desired lean angle by tilting the flywheel.

The basic task for an autonomous vehicle is to track a desired path. We propose a line following controller for the robot to track any desired line from any initial configurations. The concept of the controller is based on the motion of bicycle riding. The robot can only execute a path with curvature continuity due to the rolling constraints. We first design the linear and steering velocities for driving the robot to the desired line through controlling the path curvature. Because of the absence of a special steering mechanism such as a steering front wheel, the robot steers only by leaning itself to a predefined angle. The controller applies the linear state feedback to stabilize the robot to the predefined lean angle such that resulting steering velocity of the robot converges to the desired steering velocity. This line following controller avoids directly solving the complicated model of the robot which is subject to two nonholonomic constraints. Furthermore, the concept of this controller can also be extended to track any desired circle trajectory.

Acknowledgments

I would like to express my sincere gratitude to my supervisor Prof. Yangsheng Xu for his patience and guidance on all aspects of the work. I would like to thank the members of my committee, Prof. Yun-hui Liu and Prof. Jie Huang for their valuable and constructive suggestions thoughout.

I would like to thank my colleague, Wai-kuen Yu, for my research support and our friendship. I enjoyed especically the memory of the tough moments in the lab when we were preparing for demonstrations together.

I would like to thank H. Ben Brown for providing excellent technical support for Gyrover.

I further wish to thank Winston Sun and Wai-keng Fung, for their contributions to this thesis in the form of comments and feedback, and their excellent support with all matters related to computer usage; Dan Ding for her help in translating the abstract to the chinese version; Loi-wah Sun and Ka-keung Lee, for kindly proofreading this thesis.

Contents

List of Figures

List of Tables

Chapter 1
Introduction

1.1 Motivation

Traditionally, people consider mobile robots as quasi-static devices. Numerous robots with four, six or more wheels have been developed to maximize mobility on various terrain. (See, for example, [3] [10] [14] [19] [20].) Likewise, legged robots which may have potentially greater mobility in a rough terrain, have been built and demonstrated, such as [23], [42]. Generally these robots have featured low center-of-mass placement and broad base of support such that they are stable statically, and can tolerate large slope without rolling over. However, when the vehicles pass over bumps, they will easily roll over when moving in a relatively high speed. Dynamic disturbances at the wheels generate large torques, tending to upset the vehicle about the roll, pitch and yaw axes. This dynamic effects gain a relative importance when the speed is high, gravity is weak and dynamic disturbances (e. g. rough terrain) are great.

On the other hand, consider a bicycle or a motorcycle which has two wheels in the fore-aft (tandem) configuration. Such a vehicle is statically unstable in the roll direction, but achieves dynamic stability at moderate speed through appropriate steering geometry and gyroscopic action of the steering front wheel. Steering stability generally increases with speed due to gyroscopic effects. Dynamic forces at the wheel-ground contact point act on or near the vehicle center (sagital) plane, and thus produce minimal roll disturbances. Additionally, the bicycles have larger maneuverability than the quasti-static devices.

In order to retain dynamic and static stabilities, we designed a single wheel, gyroscopically stabilized robot (called Gyrover) as shown in Figure 1.1. Essentially, Gyrover is a sharp-edged wheel, with an actuation mechanism fitted inside the wheel. The actuation

Figure 1.1: The first prototype of Gyrover

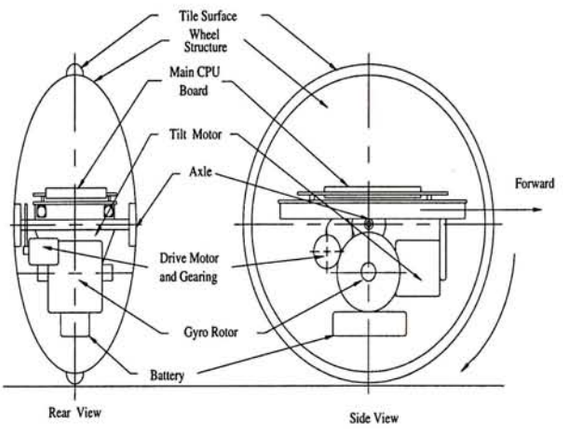

Figure 1.2: The basic configuration of Gyrover

mechanism consists of three separate actuators: (1) spin motor, which spins a suspended flywheel at a high rate, imparting dynamic stability to the robot; (2) tilt motor, which controls the steering of Gyrover; and (3) drive motor, which causes forward and/or backward acceleration, by driving the single wheel directly.

The behavior of Gyrover is based on the principle of gyroscopic precession as exhibited in the stability of a rolling wheel. Because of its angular momentum, a spinning wheel tends to precess at right angles to an applied torque, according to the fundamental equation of gyroscopic precession:

$$T = J \times \omega \times \Omega \tag{1.1}$$

where ω is the angular speed of the wheel, Ω is the wheel's precession rate, normal to the spin axis, J is the wheel polar moment of inertia about the spin axis, and T is the applied torque, normal to the spin and precession axes. Therefore, when a rolling wheel leans to one side, rather than just fall over, the gravitationally induced torque causes the wheel to precess so that it turns in the direction that it is leaning. Gyrover supplements this basic concept with the addition of an internal gyroscope — the spinning flywheel — nominally aligned with the wheel and spinning in the direction of forward motion. The flywheel's angular momentum produces lateral stability when the wheel is stopped or moving slowly. The schematic of the mechanical design is shown in Figure 1.2.

Owing to the gyroscopic effect of the spinning flywheel, the static stability of the robot

is improved. Dynamic disturbances due to surface irregularities act through or near the wheel's center of mass, producing minimal torques in roll, pitch and yaw. Furthermore, the angular momentum of the wheel, in addition to providing the natural gyroscopic steering mechanism, tends to stabilize the wheel with respect to roll and yaw. In terms of attitude control, the robot is relatively insensitive to fore/aft and side slopes. The result is a highly stable rolling motion with minimal attitude disturbances and tolerance to fore/aft and vertical disturbances. In addition to those cited above, Gyrover has a number of potential advantages over multi-wheeled vehicles:

1. The entire system can be enclosed within the wheel to provide mechanical and environmental protection for equipment and mechanisms.

2. Gyrover is resistant to getting stuck on obstacles because it has no body to hang up, no exposed appendages, and the entire exposed surface is *live* (driven).

3. The tiltable flywheel can be used to right the vehicle from its statically stable, rest position (on its side). The wheel has no "backside" on which to get stuck.

4. Gyrover can turn in place by simply leaning and precessing in the desired direction, with no special steering mechanism, enhancing maneuverability.

5. Single-point contact with the ground eliminates the need to accommodate uneven surfaces and simplifies control.

6. Full drive traction is available because all the weight is on the single drive wheel.

7. A large pneumatic tire may have very low ground-contact pressure, resulting in minimal disturbance to the surface and minimum rolling resistance. The tire may be suitable for traveling on soft soils, sand, snow or ice; riding over brush or other vegetation; or, with adequate buoyancy, for traveling on water.

Potential applications for Gyrover are numerous. Because it can travel on both land and water, it may find amphibious use on beaches or swampy areas, for general transportation, exploration, rescue or recreation. Similarly, with appropriate tread,it should travel well over soft snow with good traction and minimal rolling resistance. As a surveillance robot, Gyrover could use its slim profile to pass through doorways and narrow passages, and its

ability to turn in place to maneuver in tight quarters. Another potential application is as a high-speed lunar vehicle, where the absence of aerodynamic disturbances and low gravity would permit efficient, high-speed mobility.

The robot offers tremendous potential applications. At the same time, the robot concept also brings a number of challenging problems in modeling and control due to the following characteristics:

1. Dynamic coupling: It is a highly coupled dynamic system between the wheel and the flywheel because the flywheel is mounted on the rolling wheel through a two-link manipulator. In fact, there is no actuator directly controlling the roll angle of the robot, while the flywheel can be tilted to different orientations by a tilt motor. Thus, it is underactuated in the roll direction. This is similar to the case when a manipulator is mounted on a satellite through dynamical coupling to its free-floating base [45]. Bergerman [4] showed that DOFs of an underactuated system are usually coupled by such dynamic forces. Although the dynamic coupling complicates the system, it allows us to control the roll angle of the robot indirectly by tilting the flywheel.

2. Nonholonomic constraints: The single wheel robot is subject to two nonholonomic constraints: the first order and the second order nonholonomic constraints. The first order one arise in the robot rolling on the plane without slipping. There are numerous examples for the control of a car or an unicycle (one wheel system) with the rolling constraints such as [25] and [6], they assumed that the wheels are constrained to the vertical position. However, our robot is not constrained to the vertical position and it can have different lean angles. On the other hand, the second order constraints arise in the absence of a direct actuator in the roll direction. There are many examples for the underactuated systems [1], [28], [40],[24], and [31] .

3. Unstable in the lateral direction: The robot is similar to a single track vehicle such as a bicycle or an unicycle in that it is inherently unstable in the lateral direction because there is no direct actuation for balancing the vehicle. However, its lateral stability can be maintained during rolling because the gyroscopic torque, resulting from the coupling motion between the yaw and roll motions, balances the vehicle. Generally, change in the yaw angle (precession rate) is for the stability control of the roll angle.

Furthermore, if we choose the yaw rate as the output of the system, the system will exhibit non-minimum phase behaviour.

In this thesis, the goal is to study these fundamental characteristics in order to develop a dynamic model and control methods for the robot. We formulate the kinematics and dynamics of the robot and study its dynamic properties including the stabilization and the tilting effect of the flywheel to the robot. We linearize the developed model to study the controllability and non-minimun phase characteristic, in order to develop a linear state feedback for stabilizing the robot to the desired lean angle. We study the line following method to drive the robot to a desired line without falling.

1.2 Previous work

Since the single wheel robot is a novel concept, the model of the robot and the analysis of the system dynamics have not been studied in the past. The two main components of the robot are the sharp-edged wheel and the high speed spinning flywheel. The idea of modeling this robot is based on the model of an unicycle and a spacecraft equiped with a momentum wheel (spinning flywheel). Both Schoonwinkel [36] and Vos [41] built an autonomous unicycle in which they modeled the human-riding-unicycle system as a three-bodies system, i.e., a wheel, a frame and a rotary turntable. Schoonwinkel used the Lagrange method to formulate the linear model while Vos used the Kane's formalism. In their linear model, both of them separated the lateral and longitudinal dynamics by perturbated the yaw rate to specific quantities. Nakajima et al. [26] designed an unicycle which is similar to a rugby ball where there is a rotary actuator between the upper and lower body. They also treated the longitudinal dynamics separatly from the lateral dynamics. They modeled the longitudinal and lateral dynamics as a wheel inverse pendulum and a double inverse pendenlum respectively. In their model, they have not considered the rolling constraints and the yaw dynamics. Beznos et al. [5] studied gyroscopically stabilized bicycle consisting of two coupled gyroscopes spinning in the opposite directions. They presented a linear model of the bicycle with the coupled gyroscopes. However, the yaw dynamics of the bicycle have not been considered and the steering angle was decoupled from the dynamics. It is because

the steering front wheel can be controlled directly. For the spacecraft with the momentum wheel, Bong [43] considered the momentum wheel as an external torque generator for the spacecraft. They first derived the equations of motion of the spacecraft and momemtum wheel independently, then considered the dynamics of the momemtum wheel as the torque for the dynamics of the spacecraft.

For the stabilization of the single wheel robot, it is useful to understand the stabilization of an unicycle or a bicycle. Schoonwinkel [36] used the LQG method to stabilize the robot to the vertical position. Based on Schoonwinkel's model, Vos and Flotow [41] proposed a new LQG structure for the stabilization of the robot and dealt with the nonlinear problem of dry friction between the wheel and floor in the yaw direction. Nakajima et al. [26] proposed two different linear state feedbacks for stabilizing their robot's longitudinal and lateral motions. However, in their lateral feedback controller, it is independent of the yaw motion. Beznos et al. [5] also proposed a linear control law for stabilizing the lateral position of the bicycle. This control law is only depend on the lean angle of their robot, the precession and precession rate of the coupled gyroscopes. It is independent of the yaw rate of the bicycle because they decoupled the steering variable and yaw angle from the dynamics while the roll dynamics of the robot and flywheel dynamics were still acceleration coupling. Most researches on the stabilization of the bicycle and unicycle used the linear control methods. However, for stabilization of the underactuated manipulator, nonlinear control methods are adopted. Arai and Tachi [1] were the first to propose a 2-phase method to control all joints of the underactuated manipulator to an equilibrium position. Hauser and Murray [13] proposed a method to control the Acrobot in the neighborhood of the manifold of the inverted equilibrium positions. Papadopoulos and Dubowsky [29] proposed to control the failed joint of a space manipulator to an equilibrium point while guaranteeing that the active joints and the base would come to a rest at the end of the motion. However, the underactuated manipulators are acceleration coupling due to the existence of the off-diagonal terms in the inertial matrix between active and passive joints, while there is no acceleration coupling between the yaw and roll dynamics of the unicycle. Therefore, the control methods for the underactuated manipulators are not suitable to the unicycle although its roll direction is underactuated.

From my knowledge, no publication has been seen in the path following/trajectory tracking of an autonomous unicycle robot. A large number of researchers have proposed

methods to the path following/trajectory tracking of the mobile robot with nonholonomic constraints [6], [38], [18], [34], [9], [33] and [39]. These results, however, cannot be directly extended to the path following of the single wheel robot because the nonholonomic constraints of the ordinary mobile robot assumed that the wheel is constrained to the vertical position while the constraints of the single wheel robot allow the wheel to perturbate from the vertical position. Rui [30] proposed a controller for asymptotically path tracking of a rolling disk which is allowed to perturbate from the vertical position. However, he assumed that a torque directly acted on the roll direction of the disk for balancing. Getz [11], [12] proposed a (dynamic inversion)controller for approximately tracking a path while balancing the bicycle. In the controller, he constructed a dynamical system which is depend on the error between the reference and real trajectory of the robot and the equilibrium equation of the lean angle. The equilibrium point of the dynamical system is time varying, depending on the desired path in the plane. In order to approximatelly track the desired path with balance, the bicycle is stabilized to the lean angle which is equal to the equilibrium point of the dynamical system, using his controller. However, this controller is not suitable for the real time control because it is time consuming in calculating the value of the equilibrium point numerically.

1.3 Thesis overview

In this thesis we discuss the challenging problems related to the modeling, stabilization and path following of the single wheel robot which is nonholonomic, underactuated and nonminimum phase. The thesis is organized as follows:

- Chapter 2: **Dynamics of the Single Wheel Robot.** We derive the kinematics and dynamics of the robot. In derivation of the model, we consider the robot as a combination of three components: a wheel (rolling disk), an internal mechanism and a flywheel. We first study the kinematics and dynamics of the rolling disk. Based on the model of the rolling disk, we develop the dynamics of the robot and study its dynamic properties, including the stabilization and the tilting effect of the flywheel to the robot. Preliminary experimental results are shown for varifing the developed model.

- Chapter 3: **Stabilization of the Single Wheel Robot.** We first linearize the system around the vertical position. We investigate the controllability and non-minimum phase characteristic of the linearized system. Because of lateral instability of the robot, we propose a linear state feedback controller for stabilizing the robot to any desired lean angles when the robot is rolling with constant velocity. Owing to the absence of special steering mechanism such as a steering front wheel, the robot steers only by leaning itself to the predefined angle. Hence, we cannot control the yaw and lean angle independently. Should we ignore the roll angle in controlling the steering velocity, it will fall. On the other hand, when the robot achieves the equilibrium state, in which the accelerations in yaw, pitch and roll directions are equal to zero, the equilibrium steering rate of the robot is corresponding to one and only one lean angle, i.e., if the lean angle change, the steering rate will also change. Finally, we propose an algorithm for tracking the reference steering velocity by stabilizing the robot to an equilibrium lean angle which corresponds to that steering velocity.

- Chapter 4: **Path Following of the Single Wheel Robot.** We redefine the configuration of the robot in terms of the path curvature. We design a line following controller to track the Y-axis of the inertia frame and then extend the controller to track any desired line. We divide the line following controller into two parts:(1) velocity inputs are designed for the kinematic model to make the position and orientation error asymtotically stable. This is called velocity control law. (2) torque control law is designed such that the linear and steering velocities of the robot converge to the desired velocities obtained from the velocity control law. For the first part, we consider the derivative of the path curvature as the control law. It is expressed as a linear combination of the position error, the orientation error and the path curvature. We demonstrate the asymptotic stability of the control law. Using this control law, the smooth velocity control inputs (linear and steering velocities) are determined while the curvature continuity can be ensured. For the second part, we desire to convert the smooth velocity control inputs into a torque control for the robot. Based on the linear state feedback developed in Chapter 3, we compute the tilt torque of the flywheel for stabilizing the robot to the lean angle which is corresponding to the desired steering velocity. Fi-

nally, we investigate the effects of the initial heading angle, the rolling speed and the controller gains to the line following controller.

- Chapter 5: **Conclusion** The contributions of the thesis are summarized and a number of ideas and problems for future work are suggested.

Chapter 2

Dynamics of the Single Wheel Robot

In this chapter, we first derive the kinematics and dynamics of a disk which rolls without slipping, and then study its dynamic characteristics, such as the steady precession and the stable rolling condition. Based on the model of the rolling disk, we develop the model of the single wheel robot which is considered as a combination of three components: a wheel (rolling disk), an internal mechanism and a flywheel. They are connected by a two-link manipulator. We then simplify the model by decoupling the tilt angle of the flywheel from the dynamics. Finally, we investigate the dynamic properties of the single wheel robot, sush as the stabilization of the flywheel via simulation and experiment study.

2.1 Dynamic model of a rolling disk

The kinematics and dynamics of the single wheel robot are different from those of a unicycle (single rolling disk) developed in [6]. The difference lies in the assumption that the unicycle always remains vertical. On the contrary, the single wheel robot can be considered as a rolling disk which is not constrained to the vertical position and is connected to a high speed spinning flywheel through a two link manipulator. Therefore, it is important to model and study the dynamics of a general rolling disk system which is perturbed from the vertical position. This model can serve well as a basis for the study of a model of the single wheel robot. To this end, we first derive the kinematic constraints of the disk and then derive the equations of motion.

Consider a disk rolling without slipping on a horizontal plane as shown in Figure 2.1. Let $\Sigma_O\{X, Y, Z\}$ and $\Sigma_B\{x_B, y_B, z_B\}$ be the inertial frame whose x-y plane is anchored to the flat surface and the body coordinate frame whose origin is located at a center of the rolling disk, respectively. Let (X_c, Y_c, Z_c) be the Cartesian coordinates of the center of mass (C) with

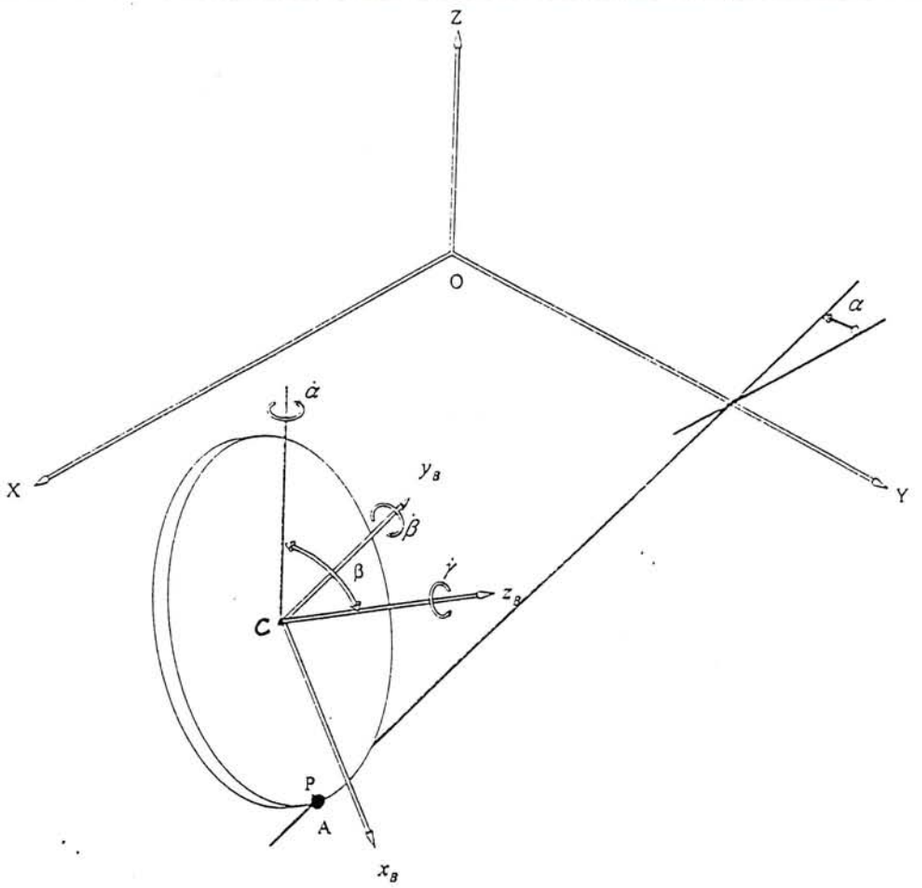

Figure 2.1: Definition of coordinate frames and system variables of a rolling disk

respect to the inertial frame Σ_O. Let P denotes the point of the contact on the disk and A denotes the point of contact on the plane. The configuration of the disk can be described by six generalized coordinates $(X_c, Y_c, Z_c, \alpha, \beta, \gamma)$, where α is the steering (precession) angle measured from the X-axis to the contact line LA, $\beta \in (0, \pi)$ is the lean (nutation) angle measured from the Z-axis to the z_B, and γ is the rolling angle.

2.1.1 Kinematic constraints

We define $(\hat{i}, \hat{j}, \hat{k})$ and $(\hat{l}, \hat{m}, \hat{n})$ be the unit vectors of the coordinate system $XYZO(\Sigma_O)$ and $x_B y_B z_B C(\Sigma_B)$, respectively. Let $S_x := \sin(x)$ and $C_x := \cos(x)$. The transformation between these two coordinate frames is given by

$$\begin{bmatrix} \hat{i} \\ \hat{j} \\ \hat{k} \end{bmatrix} = R_B^O \begin{bmatrix} \hat{l} \\ \hat{m} \\ \hat{n} \end{bmatrix} \tag{2.1}$$

where R_B^O is the rotation matrix from Σ_O to Σ_B.

$$R_B^O = \begin{bmatrix} -S_\alpha C_\beta & -C_\alpha & -S_\alpha S_\beta \\ C_\alpha C_\beta & -S_\alpha & C_\alpha S_\beta \\ -S_\beta & 0 & C_\beta \end{bmatrix} \tag{2.2}$$

Let v_c and ω_B denote the velocity of the center of mass of the disk and the angular velocity of the disk with respect to the inertia frame Σ_O. Then, we have

$$\omega_B = -\dot{\alpha} S_\beta \hat{l} + \dot{\beta} \hat{m} + (\dot{\gamma} + \dot{\alpha} C_\beta) \hat{n} \tag{2.3}$$

The constraints require that the disk rolls without slipping on the horizontal plane, i.e, the velocity of the contact point on the disk v_p is zero at any instant

$$v_p = 0, \tag{2.4}$$

Now, we can express v_c as

$$v_c = \omega_B \times r_{cp} + v_p \tag{2.5}$$

where $r_{cp} = -Rl$ representing the vector from the point P to C in Figure 2.1. Substituting Eqs. (2.3) and (2.4) in Eq. (2.5) gives

$$v_c = \dot{X}_c \hat{i} + \dot{Y}_c \hat{j} + \dot{Z}_c \hat{k}, \tag{2.6}$$

where

$$\dot{X}_c = R(\dot{\gamma} C_\alpha + \dot{\alpha} C_\alpha C_\beta - \dot{\beta} S_\alpha S_\beta) \tag{2.7}$$

$$\dot{Y}_c = R(\dot{\gamma} S_\alpha + \dot{\alpha} C_\beta S_\alpha + \dot{\beta} C_\alpha S_\beta) \tag{2.8}$$

$$\dot{Z}_c = R\dot{\beta} C_\beta \tag{2.9}$$

Eqs. (2.7) and (2.8) are nonintegrable and hence are nonholonomic, while Eq. (2.9) is integrable, i.e,

$$Z_c = R S_\beta. \tag{2.10}$$

Therefore, the rolling disk system can be represented by five (e.g. $X_c, Y_c, \alpha, \beta, \gamma$), instead of six, independent variables.

2.1.2 Equations of motion

In this section, we first formulate the Lagrangian $L = T - P$ of the disk, where T and P are the kinetic energy and potential energy of the disk respectively. We derive the equations of motion using the constrained Lagrangian method, and then eliminate the constrained generalized coordinates (X_c, Y_c) from the equations of motion.
The kinetic energy of the disk is given by,

$$\begin{aligned} T_w &= \frac{1}{2} m_w \left[\dot{X}_c^2 + \dot{Y}_c^2 + \dot{Z}_c^2\right] \\ &\quad + \frac{1}{2}\left[I_{xxw}\omega_x^2 + I_{yyw}\omega_y^2 + I_{zzw}\omega_z^2\right] \end{aligned} \tag{2.11}$$

where $I_{xxw}, I_{yyw}, I_{zzw}$ are the moment of inertia of the disk about x, y, z axes respectively, and m_w is the mass of the disk. Substituting Eqs. (2.3) and (2.10) in Eq. (2.11) yields

$$\begin{aligned} T_w &= \frac{1}{2} m_w \left[\dot{X}_c^2 + \dot{Y}_c^2 + (R\dot{\beta}C_\beta)^2\right] + \frac{1}{2}\left[I_{xxw}(\dot{\alpha}S_\beta)^2 \right. \\ &\quad \left. + I_{yyw}\dot{\beta}^2 + I_{zzw}(\dot{\alpha}C_\beta + \dot{\gamma})^2\right] \end{aligned} \tag{2.12}$$

The potential energy of the disk is

$$P_w = m_w g R S_\beta \tag{2.13}$$

Thus the Lagrangian for the rolling disk is

$$\begin{aligned} L_w &= \frac{1}{2} m_w \left[\dot{X}_c^2 + \dot{Y}_c^2 + (R\dot{\beta}C_\beta)^2\right] + \frac{1}{2}\left[I_{xxw}(\dot{\alpha}S_\beta)^2 \right. \\ &\quad \left. + I_{yyw}\dot{\beta}^2 + I_{zzw}(\dot{\alpha}C_\beta + \dot{\gamma})^2\right] - m_w g R S_\beta \end{aligned} \tag{2.14}$$

Using the constrained Lagrangian method,

$$\frac{d}{dt}\frac{\partial L}{\partial \dot{q}_j} - \frac{\partial L}{\partial q_j} = \sum_{s=1}^{m-n} \lambda_s A_{sj}, j \in \{1, 2, ..., m-n\} \tag{2.15}$$

where q_j is the jth generalized coordinates and λ_s is the s^{th} lagrangian multiplier. The equations of motion of the rolling disk without actuation is

$$M(q)\ddot{q} + N(q, \dot{q}) = A^T \lambda \tag{2.16}$$

where $M(q) \in \mathcal{R}^{5\times5}$ and $N(q, \dot{q}) \in \mathcal{R}^{5\times1}$ are the inertia matrix and nonlinear term respectively.

$$A(q) = \begin{bmatrix} 1 & 0 & -RC_\alpha C_\beta & RS_\alpha S_\beta & -RC_\alpha \\ 0 & 1 & -RC_\beta S_\alpha & -RC_\alpha S_\beta & -RS_\alpha \end{bmatrix} \tag{2.17}$$

$$q = \begin{bmatrix} X_c, & Y_c, & \alpha, & \beta, & \gamma \end{bmatrix}^T, \lambda = \begin{bmatrix} \lambda_1, & \lambda_2 \end{bmatrix}^T$$

The nonholonomic constraints can be written as,

$$A(\dot{q})\dot{q} = 0. \tag{2.18}$$

Now, we will eliminate the Lagrange multipliers so that a minimum set of differential equations is obtained[6]. We first partition the matrix $A(q)$ into A_1 and A_2 where $A = [A_1|A_2]$

$$A_1 = \begin{bmatrix} 1 & 0 \\ 0 & 1 \end{bmatrix}, A_2 = \begin{bmatrix} -RC_\alpha C_\beta & RS_\alpha S_\beta & -RC_\alpha \\ -RC_\beta S_\alpha & -RC_\alpha S_\beta & -RS_\alpha \end{bmatrix}$$

Let

$$C(q) = \begin{bmatrix} -A_1^{-1}A_2 \\ I_{3\times 3} \end{bmatrix} \tag{2.19}$$

Then consider the following relationship

$$\dot{q} = C(q)\dot{q}_2 \tag{2.20}$$

where $q_1 = [X_c, Y_c]^T$ and $q_2 = [\alpha, \beta, \gamma]^T$. Differentiating Eq. (2.20) yields

$$\ddot{q} = C(q)\ddot{q}_2 + \dot{C}(q)\dot{q}_2 \tag{2.21}$$

Substituting Eq. (2.21) into Eq. (2.16) and premultiplying both sides by $C^T(q)$ gives

$$\begin{aligned} &C^T(q)M(q)C(q)\ddot{q}_2 \\ &= C^T(q)\left[-N(q, C(q)\dot{q}_2) - M(q)\dot{C}(q)\dot{q}_2\right] \end{aligned} \tag{2.22}$$

where $C^T(q)M(q)C(q)$ is a 3×3 symmetric positive definite matrix function. Note that *Eq.(2.22) depends only on* (α, β, γ). By numerical integration, we can obtain q_2 and $\dot{q}_2$ from $\ddot{q}_2$ in Eq. (2.22), and then obtain (X_c, Y_c) by substituting q_2 and $\dot{q}_2$ in Eq. (2.20). The resulting equations of motion are

$$\bar{M}(q)\ddot{q} = \bar{N}(q, \dot{q}) \tag{2.23}$$

where $q = [\alpha, \beta, \gamma]^T$,

$$\begin{aligned}
\bar{M}(q) &= C^T(q)M(q)C(q) \\
&= \begin{bmatrix} I_{xxw} + I_{xxw}C_\beta^2 + mR^2C_\beta^2 & 0 & 2I_{xxw}C_\beta + mR^2C_\beta \\ 0 & I_{xxw} + mR^2 & 0 \\ 2I_{xxw}C_\beta + mR^2C_\beta & 0 & 2I_{xxw} + mR^2 \end{bmatrix},
\end{aligned}$$

$$\begin{aligned}
\bar{N}(q, \dot{q}) &= C^T(q)\left[-N(q, C(q)\dot{q}_2) - M(q)\dot{C}(q)\dot{q}_2\right] \\
&= \begin{bmatrix} (I_{xxw} + mR^2)S_{2\beta}\dot{\alpha}\dot{\beta} + 2I_{xxw}S_\beta\dot{\beta}\dot{\gamma} - \mu_s\dot{\alpha} \\ -gmRC_\beta - (I_{xxw} + mR^2)C_\beta S_\beta\dot{\alpha}^2 - (2I_{xxw} + mR^2)S_\beta\dot{\alpha}\dot{\gamma} \\ -2(I_{xxw} + mR^2)S_\beta\dot{\alpha}\dot{\beta} \end{bmatrix}.
\end{aligned}$$

$\bar{M}(q) \in \mathcal{R}^{3\times3}$ and $\bar{N}(q, \dot{q}) \in \mathcal{R}^{3\times1}$ are the inertial matrix and nonlinear term respectively. Eqs. (2.7), (2.8) and Eq. (2.23) form the nonholonomic velocity constraints and the reduced dynamic model of the rolling risk, respectively. Note that if the lean angle β is set to be 0° or 180°, the disk falls on the ground, its inertial matrix $\bar{M}$ will become singular because it violates the assumption of rolling without slipping.

2.1.3 Characteristics of the rolling disk

Steady Precession

It is interesting that although the rolling disk is perturbated from the vertical position, it still does not fall because a gyroscopic torque, resulting from the coupling motion between the roll and yaw motions, balances the gravitational torque. The special case of this phenomena is the steady precession, in which the lean rate $\dot{\beta}$ is equal to zero, such that the center C (Figure 2.1) can follow a circular path with a constant precession rate $\dot{\alpha}_s$. Here we derive the steady precession rate $\dot{\alpha}_s$ of the rolling disk as a function of the lean angle β and the radius of path curvature. Let ρ be the radius of curvature of that path, and let the center of the path be situated on Z-axis. Then we define the coordinates of point C as

$$X_c = -\rho\sin\alpha, \quad Y_c = \rho\cos\alpha$$

Because the lean angle β keeps constant, from Eq. (2.10), Z_c is also fixed. Then solving the constraints Eqs. (2.7) and (2.8) with $\dot{\beta} = 0$, the resulting equation is

$$\dot{\gamma} = -\dot{\alpha}\left[\frac{\rho}{R} + C_\beta\right]. \tag{2.24}$$

Substituting Eq. (2.24) into Eq. (2.23) with $\dot{\beta} = 0$. $\ddot{\alpha}$ and $\ddot{\gamma}$ become zero, and yields the steady precession rate as

$$\dot{\alpha}_s = \sqrt{\frac{-m_w g R C_\beta}{(I_{xxw} + m_w R^2)C_\beta S_\beta - (2I_{xxw} + m_w R^2)S_\beta(\frac{\rho}{R} + C_\beta)}} \tag{2.25}$$

Figure 2.2 shows the simulation results of a rolling disk ($m_w = 2\ kg,\ R = 0.15m$), under the initial conditions:

$$\begin{cases} \beta = 70^o, \alpha = \gamma = 0^o, \\ \dot{\beta} = 0\ rad/s, \dot{\alpha} = \dot{\alpha}_s = 1.48\ rad/s, \dot{\gamma} = \dot{\gamma}_s = -15.5715\ rad/s, \\ X_c = 0, Y_c = 5R, \rho = 5R. \end{cases}$$

It shows that the disk can follow the circle with the radius of 5R if the initial conditions follow the conditions in Eqs. (2.24) and (2.25). Futhermore, the precession rate $\dot{\alpha}$ and lean angle β always keep constant. However, if one of the initial conditions does not follow the conditions in Eqs. (2.24) and (2.25). The resulting trajectory will deviate from the desired one. Its precession rate $\dot{\alpha}$ and lean angle β is no longer fixed. The simulation result is shown in Figure 2.3, with the initial lean angle β and lean rate $\dot{\beta}$ are equal to $\frac{\pi}{4}$ and $\frac{\dot{\alpha}_s}{3}$ respectively, while the other conditions are consistent with the previous simulation.

Stable rolling condition

The rolling speed of the rolling disk is important for the stability of the motion when external disturbances exist. Here, we present the minimum rolling speed for the disk such that the error dynamics is stable. Assume a slight disturbance (by nonsmooth griund surface) is imported to a rolling motion when the disk is upright, i.e., $\beta = \frac{\pi}{2} + \varepsilon$, where ε is the small perturbation angle in the roll direction. Thus, the precession rate $\dot{\alpha}$ is no longer zero, although it remains a small quantity. Hence,

$$\dot{\beta} = \dot{\varepsilon},\ \dot{\alpha}\ is\ small.$$

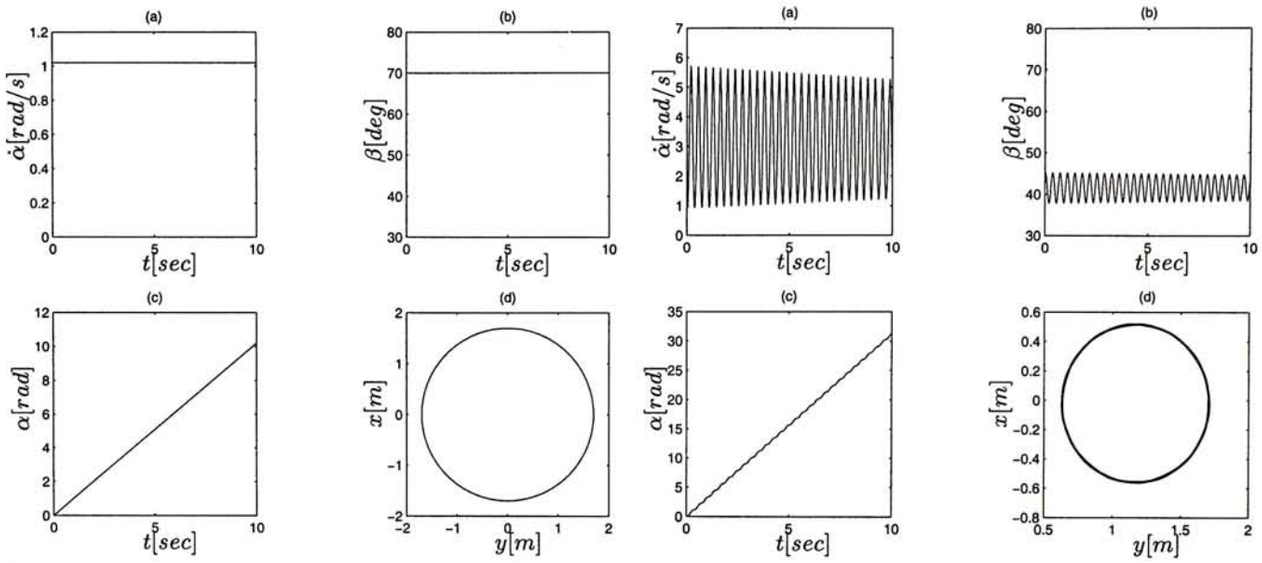

Figure 2.2: The simulation results of the rolling disk with nominal steady precession

Figure 2.3: The simulation results of the rolling disk with initial conditions deviated from the nominal steady precession.

Then the equations of motion (roll dynamics) becomes

$$(I_{xxw} + m_w R^2)\ddot{\varepsilon} + \left[(I_{zzw} + m_w R^2)\frac{I_{zzw}\dot{\gamma}^2}{I_{xxw}} - m_w g R\right]\varepsilon = 0 \tag{2.26}$$

Note that Eq. (2.26) become an unstable dynamics if $\left[(I_{zzw} + mR^2)\frac{I_{zzw}\dot{\gamma}^2}{I_{xxw}} - mgR\right] < 0$, so that the ε will diverge. The minimum rolling speed for the rolling disk to have a stable motion is

$$\dot{\gamma}_{min} = \sqrt{\frac{I_{xxw} m_w g R}{I_{zzw}(I_{zzw} + R^2 m_w)}} = \sqrt{\frac{gR}{3}}, \tag{2.27}$$

where $I_{xxw} = \frac{1}{2}I_{zzw} = \frac{1}{2}m_w R^2$. Figures 2.4 and 2.5 show the results of the rolling disk with $\dot{\gamma} = 3.5\ rad/s < \dot{\gamma}_{min}$ and $\dot{\gamma} = 6\ rad/s > \dot{\gamma}_{min}$ respectively. In Figure 2.4, because the rolling speed $\dot{\gamma}$ is lower than the minimun rolling speed $\dot{\gamma}_{min}$, the perturbed roll angle ε will diverge such that the disk does not roll upright after 15 sec, resulting in an unpredictable trajectory. In Figure 2.5, the disk can keep in an upright position ($\beta = \frac{\pi}{2}$) because the rolling speed $\dot{\gamma}$ is greater than the minimun rolling speed $\dot{\gamma}_{min}$, resulting in the convergence of the perturbed roll angle ε.

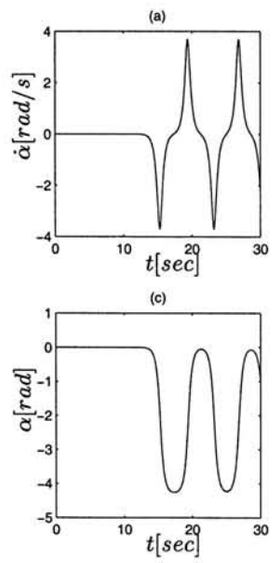

Figure 2.4: The simulation results of the rolling disk with $\dot{\gamma} = 3.5\ rad/s$

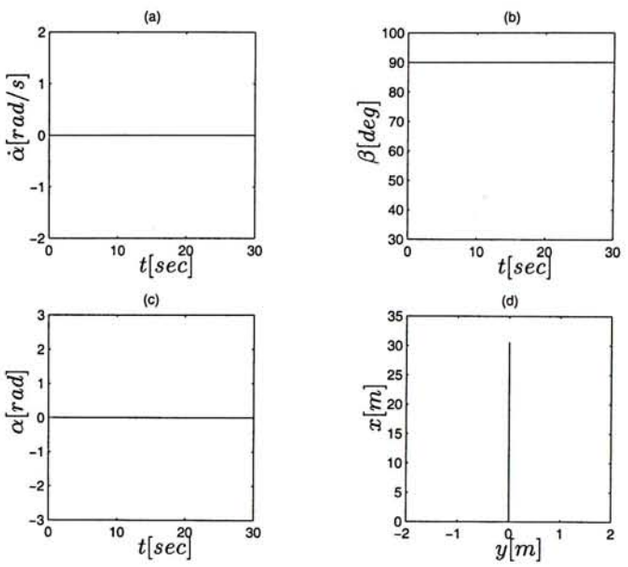

Figure 2.5: The simulation results of the rolling disk with $\dot{\gamma} = 6\ rad/s$

2.2 Dynamic model of the single wheel robot

In derivation of the dynamics of the single wheel robot, we model it as a combination of three components, including a wheel, an internal mechanism[1] and a flywheel. Variable definition of the system are shown in Figures 2.6, 2.7 and 2.8.

1. Wheel - is considered as a rigid, homogeneous disk which rolls over a perfectly flat surface without slipping. (rolling disk)

2. Internal mechanism - is considered as a point mass D which connects to the center of the wheel c through a massless link l_1. It is allowed to swing on the plane perpendicular to the rotating axis of the wheel through l_1.

3. Flywheel - is considered as a thin disk which connects to the point mass D through a massless link l_2. It can be tilted about the y_c-axis through l_2 and spinned about the z_a-axis.

[1]The equipment inside the wheel except the flywheel

2.2.1 Coordinate frames and generalized coordinates

The frame defined in Section 2.1 and the generalized coordinates $(X_c, Y_c, \alpha, \beta, \gamma)$ are necessary to describe the configuration of the wheel.

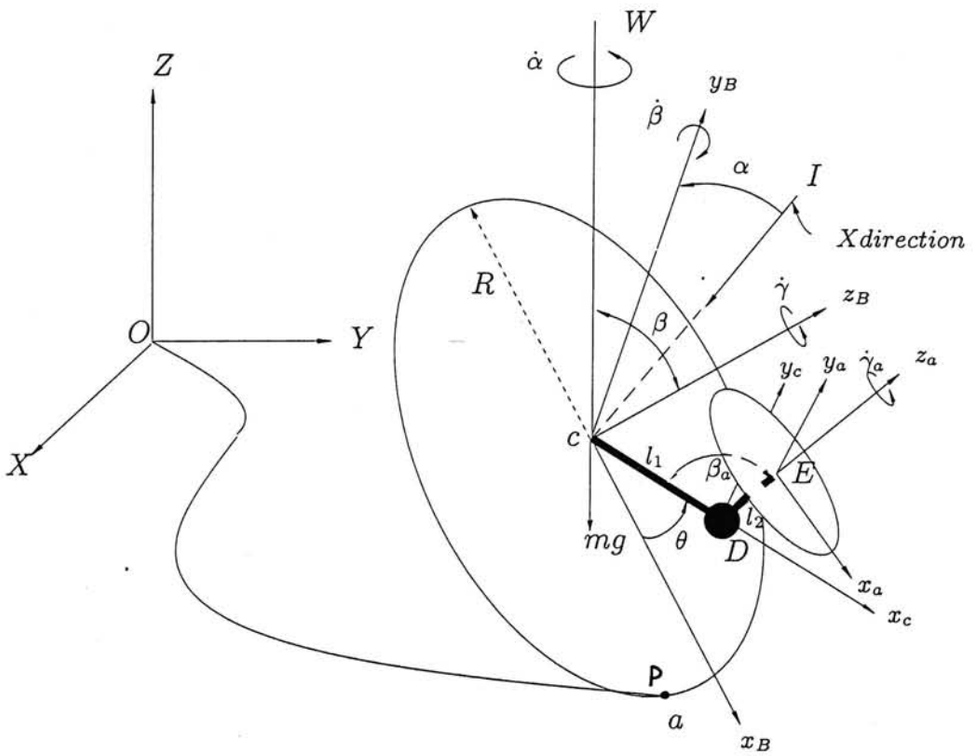

Figure 2.6: Definition of coordinate frames and system variables of the robot model

The single wheel robot has more degrees of freedom than a rolling disk, owing to the swinging motion of the link l_1 and the tilting motion of the flywheel. In addition to the two frame we defined (1) the inertial frame and (2) the body frame, we defined two more frames: (3) the coordinate frame of internal mechanism Σ_D $\{x_c, y_c, z_c\}$, whose center is located at point D and whose z-axis is always parallel to z_B, and (4) the flywheel coordinates frame Σ_E $\{x_a, y_a, z_a\}$ which located in the center of the flywheel, and its z-axis represents the axis of rotation of the flywheel. Link l_1 is rotated about the z_B-axis by a swing angle, θ. The swing angle is zero when link l_1 is parallel to x_B axis. The flywheel is tilted about the y_c-axis by the tilt angle, $\beta_a \in (0, \pi)$. Note that y_a is always parallel to y_c. Therefore, the configuration of the single wheel robot can be described by seven generalized coordinates $(X_c, Y_c, \alpha, \beta, \gamma, \theta, \beta_a)$. A summary of the definition of model variables is shown in Table 2.1.

The spinning rate of the flywheel always keeps constant because it is reluctance to change

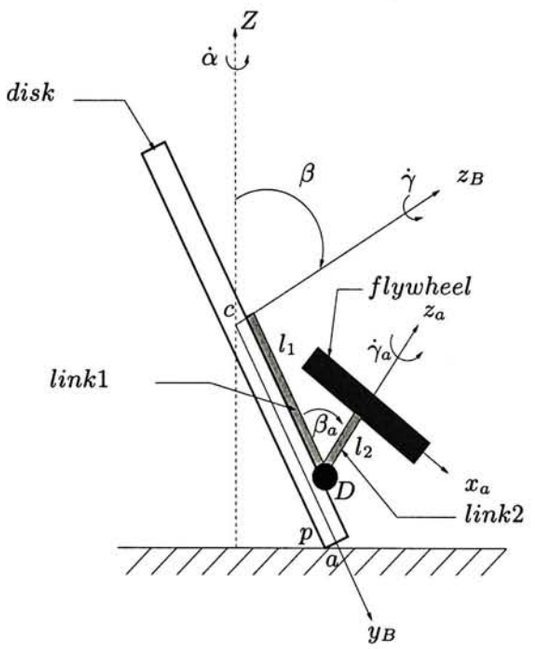

Figure 2.7: The side view of the robot model

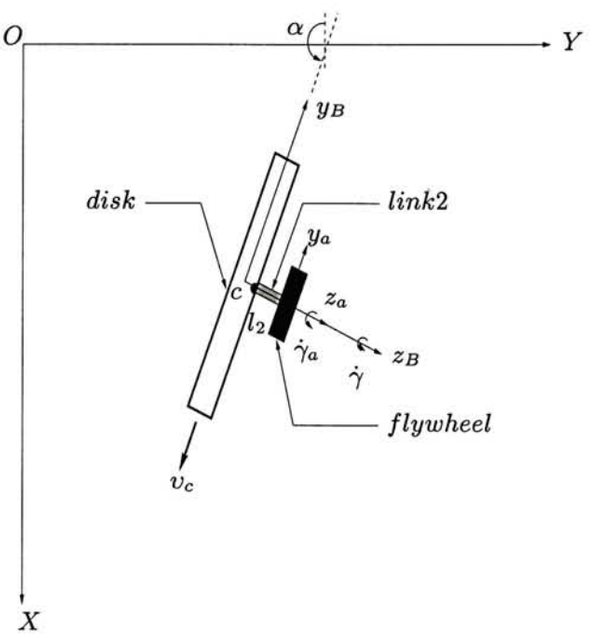

Figure 2.8: The top view of the robot model

Table 2.1: Variable definition

α, α_a	Precession angles of the wheel and flywheel, respectively, measured about the vertical axis
β	Lean angles of the wheel
β_a	Tilt angle between the link l_1 and z_a-axis of the flywheel
γ, γ_a	Spin angles of the wheel and the flywheel, respectively
θ	Angle between link l_1 and x_B-axis of the wheel
m_w, m_i, m_f	Mass of the wheel, internal mechanism and flywheel respectively
m	Total mass of the robot
R, r	Radius of the wheel and the flywheel respectively
$I_{xxw}, I_{yyw}, I_{zzw}$	Moment of inertia of the wheel about x, y and z axes
$I_{xxf}, I_{yyf}, I_{zzf}$	Moment of inertia of the flywheel about x, y and z axes
μ_s, μ_g	Friction coefficient in yaw and pitch directions, respectively
u_1, u_2	Drive torque of the drive motor and tilt torque of the tilt motor, respectively

the spinning rate due to the large moment of inertia, thus torque acting on the spin motor can be approximately constant. In this case, we only need to consider two generalized forces acting on the single wheel robot: (1) the drive torque (u_1) for controlling the rotating speed of the wheel $\dot{\gamma}$, (2) the tilt torque (u_2) for tilting the flywheel to different tilt angle β_a.

Among the three components of the robot model, only the wheel is in contact with the ground at all times Therefore the velocity constraints for the robot are the same as the non-holonomic constraints of the rolling disk. (Eqs. (2.7) and (2.8))

2.2.2 Equations of motion

In this section, the reduced equations of motion for the single wheel robot will be derived, following the procedure in Section 2.1.2. We first present the Lagrangian of each components of the robot model in the following sections. Then we present the Lagrangian of the overall system and derive the motion equations of the robot.

Wheel

We consider the wheel as a rolling disk, the Lagrangian of the wheel is the same as the rolling disk,

$$\begin{aligned} L_w &= \frac{1}{2}m_w\left[\dot{X}_c^2 + \dot{Y}_c^2 + (R\dot{\beta}C_\beta)^2\right] + \frac{1}{2}\left[I_{xxw}(\dot{\alpha}S_\beta)^2 \right. \\ &\quad \left. + I_{yyw}\dot{\beta}^2 + I_{zzw}(\dot{\alpha}C_\beta + \dot{\gamma})^2\right] - m_w g R S_\beta, \end{aligned} \tag{2.28}$$

where L_w is the Lagrangian of the wheel.

Internal mechanism

We first compute the translational and rotational parts of kinetic energy for the internal mechanism (point mass D). Let $\{x_D, y_D, z_D\}$ be the center of mass of the internal mechanism D with respect to Σ_O. The transformation from the center of mass of the wheel to the point D can be described:

$$\begin{bmatrix} x_D \\ y_D \\ z_D \end{bmatrix} = \begin{bmatrix} X_c \\ Y_c \\ Z_c \end{bmatrix} + R_B^O \begin{bmatrix} l_1 C_\theta \\ l_1 S_\theta \\ 0 \end{bmatrix} \tag{2.29}$$

Let T_i^t denote the translational kinetic energy of the internal mechanism:

$$T_i^t = \frac{1}{2} m_i [\dot{x}_D^2 + \dot{y}_D^2 + \dot{z}_D^2] \tag{2.30}$$

Differentiating Eq. (2.29) and substituting it in Eq. (2.30), we obtain T_i^t. We observed that the internal mechanism swings slowly, so that the motion should not contribute to the rotational kinetic energy substantially. Let ω_i be the angular velocity of the internal mechanism wth respect to Σ_O. We then have

$$\omega_i = R_B^D \omega_B \tag{2.31}$$

where R_B^D is the transformation from Σ_B to Σ_D.

$$R_B^D = \begin{bmatrix} C_\theta & S_\theta & 0 \\ -S_\theta & C_\theta & 0 \\ 0 & 0 & 1 \end{bmatrix} \tag{2.32}$$

The rotational kinetic energy of the internal mechanism is now given by

$$T_i^r = \frac{1}{2} \left[(\omega_{ix})^2 I_{xxi} + (\omega_{iy})^2 I_{yyi} + (\omega_{iz})^2 I_{zzi} \right] \tag{2.33}$$

The link l_1 is assumed to be massless, the principle moments of inertia of D with respect to the center c are $I_{xxi} = I_{yyi} = I_{zzi} = m_i l_1^2$. The potential energy of the internal mechanism is

$$P_i = m_i (R S_\beta - l_1 C_\theta S_\beta) \tag{2.34}$$

The Lagrangian of the internal mechanism is

$$L_i = (T_i^t + T_i^r) - P_i. \tag{2.35}$$

Flywheel

We assume that the link l_2 is very small compared to l_1,

$$l_2 \simeq 0 \tag{2.36}$$

Thus, the flywheel's center of mass (E) coincides with that of the internal mechanism (D). Therefore, the translational part of kinetic energy of the flywheel will be identical to that of the internal mechanism. Let T_f^t denote the translational kinetic energy of the flywheel, then

$$T_f^t = \frac{1}{2} m_f \left[(\omega_{ix})^2 I_{xxi} + (\omega_{iy})^2 I_{yyi} + (\omega_{iz})^2 I_{zzi} \right]. \tag{2.37}$$

Let ω_f be the angular velocity of the flywheel with respect to Σ_O. We then have

$$\omega_f = R_B^E \omega_B + \begin{bmatrix} 0 \\ \dot{\beta}_a \\ \dot{\gamma}_a \end{bmatrix} \tag{2.38}$$

where R_B^E is the transformation from Σ_B to Σ_E.

$$R_B^E = \begin{bmatrix} C_\theta S_{\beta_a} & -S_\theta S_{\beta_a} & C_{\beta_a} \\ S_\theta & C_\theta & 0 \\ C_\theta C_{\beta_a} & -C_{\beta a} S_\theta & S_{\beta_a} \end{bmatrix} \tag{2.39}$$

The rotational kinetic energy of the flywheel is now given by,

$$T_f^r = \frac{1}{2}\left[(\omega_{fx})^2 I_{xxf} + (\omega_{fy})^2 I_{yyf} + (\omega_{fz})^2 I_{zzf}\right] \tag{2.40}$$

The flywheel is assumed to be a uniform disk, the principle moments of inertia are $I_{xxf} = I_{yyf} = \frac{1}{4} m_f r^2, I_{zzf} = \frac{1}{2} m_f r^2$. The potential energy of the flywheel is

$$P_f = m_f (R S_\beta - l_1 C_\theta S_\beta) \tag{2.41}$$

The Lagrangian of the flywheel is

$$L_f = (T_f^t + T_f^r) - P_f \tag{2.42}$$

Lagrangian of the overall system

The Lagrangian of the overall system thus is

$$L \;=\; [L_w + L_i + L_f] \tag{2.43}$$

Substituting Eqs. (2.28), (2.30), (2.34), (2.40) and (2.41) in Eq. (2.43), we may determine L. There are only two control torques available on the system. The first is the drive torque (u_1) and the second is the tilt torque (u_2). Consequently, using the constrained Lagrangian method, the dynamic equation of the entire system is given by

$$M(q)\ddot{q} + N(q, \dot{q}) = A^T \lambda + Bu \tag{2.44}$$

where $M(q) \in \mathcal{R}^{7\times7}$ and $N(q,\dot{q}) \in \mathcal{R}^{7\times1}$ are the inertia matrix and nonlinear term respectively.

$$A(q) = \begin{bmatrix} 1 & 0 & -RC_\alpha C_\beta & RS_\alpha S_\beta & -RC_\alpha & 0 & 0 \\ 0 & 1 & -RC_\beta S_\alpha & -RC_\alpha S_\beta & -RS_\alpha & 0 & 0 \end{bmatrix} \tag{2.45}$$

$$q = \begin{bmatrix} X_c \\ Y_c \\ \alpha \\ \beta \\ \gamma \\ \beta_a \\ \theta \end{bmatrix}, \lambda = \begin{bmatrix} \lambda_1 \\ \lambda_2 \end{bmatrix}, B = \begin{bmatrix} 0 & 0 \\ 0 & 0 \\ 0 & 0 \\ 0 & 0 \\ k_1 & 0 \\ 0 & 1 \\ k_2 & 0 \end{bmatrix}, u = \begin{bmatrix} u_1 \\ u_2 \end{bmatrix}$$

The nonholonomic constraints can be written as,

$$A(\dot{q})\dot{q} = 0. \tag{2.46}$$

Noted that *all elements of the last two columns of the matrix A are zero*, because the nonholonomic constraints only restrict the motion of the wheel, not the flywheel. The last two columns represent the motion variables of the flywheel. Moreover, *the matrix B has only three rows with non-zero elements*, since the input torques only drive the tilt angle of the flywheel (β_a) and the rotating angle of the wheel (γ), so that the fifth and the sixth rows of B are non-zero as they represent the tilting motion of the flywheel and the rotating motion of the wheel respectively. Furthermore, when the wheel rotates, the pendulum motion of the internal mechanism is introduced, thus θ changes. Therefore, the drive torque of the wheel will also affect the pendulum motion of the internal mechanism (θ), so that the seventh row of the matrix B is not zero.

2.2.3 Model simplification

Practically, we may assume l_1 and l_2 are zero, thus the mass center of flywheel and the internal mechanism are coincident with the center of the robot. For steady motion of the robot, the pendulum motion of the internal mechanism is sufficiently small to be neglected, thus θ is set to be zero. The spinning rate of the flywheel $\dot{\gamma}_a$ is set to be constant. Let $S_{\beta,\beta_a} := sin(\beta + \beta_a)$, $C_{\beta,\beta_a} := cos(\beta + \beta_a)$, and $S_{2\beta\beta_a} := sin[2(\beta + \beta_a)]$. Based on the

previous derivation, the *normal form* of the dynamic model is

$$\bar{M}(q)\ddot{q} = \bar{F}(q,\dot{q}) + Bu \tag{2.47}$$

where $q = [\alpha, \beta, \gamma, \beta_a]^T$,

$$\bar{M} = \begin{bmatrix} \bar{M}_{11} & 0 & \bar{M}_{13} & 0 \\ 0 & I_{xxf} + I_{xxw} + mR^2 & 0 & I_{xxf} \\ \bar{M}_{13} & 0 & 2I_{xxw} + mR^2 & 0 \\ 0 & I_{xxf} & 0 & I_{xxf} \end{bmatrix},$$

$$\bar{F} = [\bar{F}_1, \bar{F}_2, \bar{F}_3, \bar{F}_4]^T,$$

$$B = \begin{bmatrix} 0 & 0 & 1 & 0 \\ 0 & 0 & 0 & 1 \end{bmatrix}^T, u = \begin{bmatrix} u1 \\ u2 \end{bmatrix}$$

$$\begin{aligned}
\bar{M}_{11} &= I_{xxf} + I_{xxw} + I_{xxw}C_\beta^2 + mR^2C_\beta^2 + I_{xxf}C_{\beta,\beta_a}^2 \\
\bar{M}_{13} &= 2I_{xxw}C_\beta + mR^2C_\beta \\
\bar{F}_1 &= (I_{xxw} + mR^2)S_{2\beta}\dot{\alpha}\dot{\beta} + I_{xxf}S_{2\beta\beta_a}\dot{\alpha}\dot{\beta} + I_{xxf}S_{2\beta\beta_a}\dot{\alpha}\dot{\beta}_a \\
&\quad +2I_{xxw}S_\beta\dot{\beta}\dot{\gamma} + 2I_{xxf}S_{\beta,\beta_a}\dot{\beta}\dot{\gamma}_a + 2I_{xf}S_{\beta,\beta_a}\dot{\beta}_a\dot{\gamma}_a - \mu_s\dot{\alpha} \\
\bar{F}_2 &= -gmRC_\beta - (I_{xxw} + mR^2)C_\beta S_\beta\dot{\alpha}^2 - I_{xxf}C_{\beta,\beta_a}S_{\beta,\beta_a}\dot{\alpha}^2 \\
&\quad -(2I_{xxw} + mR^2)S_\beta\dot{\alpha}\dot{\gamma} - 2I_{xxf}S_{\beta,\beta_a}\dot{\alpha}\dot{\gamma}_a \\
\bar{F}_3 &= 2(I_{xxw} + mR^2)S_\beta\dot{\alpha}\dot{\beta} \\
\bar{F}_4 &= -I_{xxf}C_{\beta,\beta_a}S_{\beta,\beta_a}\dot{\alpha}^2 - 2I_{xxf}S_{\beta,\beta_a}\dot{\alpha}\dot{\gamma}_a
\end{aligned}$$

where $\bar{M}(q) \in R^{4\times4}$ and $\bar{F}(q,\dot{q}) \in R^{4\times1}$ are the inertial matrix and nonlinear term of the single wheel robot respectively.

We further simplify the model by decoupling the tilting variable β_a from Eq. (2.47). Practically, β_a is directly controlled by the tilt motor (position control), assuming that the tilt actuator has an adequate torque to track the desired $\beta_a(t)$ trajectory exactly. Furthermore, there is an acceleration coupling between the lean angle and tilt angle in the roll dynamics, but $\bar{M}_{22}$ is much larger than the I_{xxf}, so that the acceleration effect of the tilt angle to the roll dynamics can be neglected. Therefore, β_a can be decoupled from Eq. (2.47). It is similar to

the case of decoupling the steering variable from the bicycle dynamics shown in [5],[11].

As we consider $\dot{\beta}_a$ as a new input u_{β_a}, the dynamics model Eq. (2.47) becomes

$$\begin{aligned} \dot{\beta}_a &= u_{\beta_a} \\ \tilde{M}(\tilde{q})\ddot{\tilde{q}} &= \tilde{F}(\tilde{q}, \dot{\tilde{q}}) + \tilde{B}\tilde{u}. \end{aligned} \tag{2.48}$$

with $\tilde{q} = [\alpha, \beta, \gamma]^T$,

$$\tilde{M} = \begin{bmatrix} \tilde{M}_{11} & 0 & \tilde{M}_{13} \\ 0 & I_{xxf} + I_{xxw} + mR^2 & 0 \\ \tilde{M}_{13} & 0 & 2I_{xxw} + mR^2 \end{bmatrix}$$

$$\tilde{F} = \left[\tilde{F}_1, \tilde{F}_2, \tilde{F}_3\right]^T$$

$$\tilde{B} = \begin{bmatrix} 0 & 0 & 1 \\ \tilde{B}_{12} & 0 & 0 \end{bmatrix}^T, \tilde{u} = \begin{bmatrix} u_1 \\ u_{\beta_a} \end{bmatrix}$$

$$\begin{aligned} \tilde{M}_{11} &= \bar{M}_{11}, \\ \tilde{M}_{13} &= \bar{M}_{13}, \\ \tilde{F}_1 &= (I_{xxw} + mR^2)S_{2\beta}\dot{\alpha}\dot{\beta} + I_{xxf}S_{2\beta\beta_a}\dot{\alpha}\dot{\beta} \\ &\quad -2I_{xxw}S_{\beta}\dot{\beta}\dot{\gamma} + 2I_{xxf}S_{\beta,\beta_a}\dot{\beta}\dot{\gamma}_a - \mu_s\dot{\alpha}, \\ \tilde{F}_2 &= \bar{F}_2, \\ \tilde{F}_3 &= \bar{F}_3, \\ \tilde{B}_{12} &= I_{xxf}S_{2\beta\beta_a}\dot{\alpha} + 2I_{xxf}S_{\beta,\beta_a}\dot{\gamma}_a, \end{aligned}$$

Eq. (2.48) shows the reduced dynamic model of the single wheel robot after decoupling the tilting varible β_a , with new matrices $\tilde{M}(\tilde{q}) \in \mathcal{R}^{3\times3}$ and $\tilde{F}(\tilde{q}, \dot{\tilde{q}}) \in \mathcal{R}^{3\times1}$. The realistic geometric/mass parameters are shown in Table 2.2 . Note that if the lean angle β is set to be 0° or 180°, the inertial matrix $\tilde{M}$ will become singular as in the case of the rolling disk. Also, the lean angle β does not couple with the rolling angle γ and the steering angle α in acceleration level, while they are coupling in velocity level through the cross terms $\dot{\alpha}$ and $\dot{\beta}$. It is different from typical underactuated systems such as the underactuated manipulators because most of them are subjected on acceleration coupling. More discussions are given in the next chapter.

Table 2.2: Parameters used in simulation and experiments

Wheel	:	$m = 1.25kg,\ R = 17cm$
Internal mechanism:		$m_i = 4.4kg,$
Flywheel	:	$m_f = 2.4kg,\ r = 5cm$
Friction coefficients:		$\mu_s = 1Nm/(rad/s),\ \mu_g = 0.01Nm/(rad/s)$

2.3 Dynamic properties of the single wheel robot

The robot dynamic model is highly coupled, nonholonomic and underactuacted. Because the major part of the robot is a rolling disk, therefore it processes a typical manner of a rolling disk. For a rolling disk, it does not fall when it is rolling, because there is a gyroscopic torque, resulting from the coupling motion between the roll and yaw motions, for balancing the gravitational torque. However, its rolling speed must be high enough to provide a sufficient gyroscopic torque for balancing the disk. When we installed a flywheel on the wheel, the robot's gyroscopic torque is greater and less depends on its rolling speed $\dot{\gamma}$, owing to the high speed spinning flywheel. That is the lean angle of the robot tends to remain unchanged. We can explain this characteristics based on the equilibrium solution of Eq. (2.48). For the low yaw rate and $\ddot{\alpha} = \ddot{\beta} = \ddot{\gamma} = 0, \dot{\beta} = 0, u_1 = u_{\beta_a} = 0$, Eq. (2.48) becomes

$$0 = gmRC_\beta + (2I_{xxw} + mR^2)S_\beta \dot{\alpha}\dot{\gamma} + 2I_{xxf}S_{\beta,\beta_a}\dot{\alpha}\dot{\gamma}_a, \tag{2.49}$$

From Eq. (2.49), the terms $\dot{\gamma}\dot{\alpha}$ and $\dot{\gamma}_a\dot{\alpha}$ are used to cancel the gravitational torques $gmRC_\beta$, in order to stabilize the roll component of the system. Because the spinning rate $\dot{\gamma}_a$ is very high, the term $2I_{xxf}S_{\beta,\beta_a}\dot{\alpha}\dot{\gamma}_a$ is significantly large, in order to cancel the gravitational torque, even though the rolling speed $\dot{\gamma}$ is low. Thus, it will achieve an equilibrium steering rate $\dot{\alpha}_s$,

$$\dot{\alpha}_s = \frac{-gmRC_{\beta_s}}{2I_{xxf}S_{\beta_s,\beta_a}\dot{\gamma}_a + (2I_{xxw} + mR^2)S_{\beta_s}\dot{\gamma}} \tag{2.50}$$

for a specific lean angle β_s.

Figures 2.9 and 2.10 show the simulation results of a rolling disk without the flywheel,

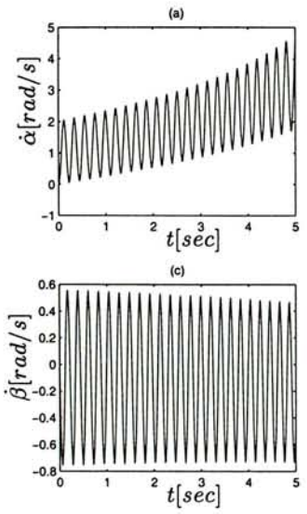

Figure 2.9: The simulation results of a rolling disk without flywheel.

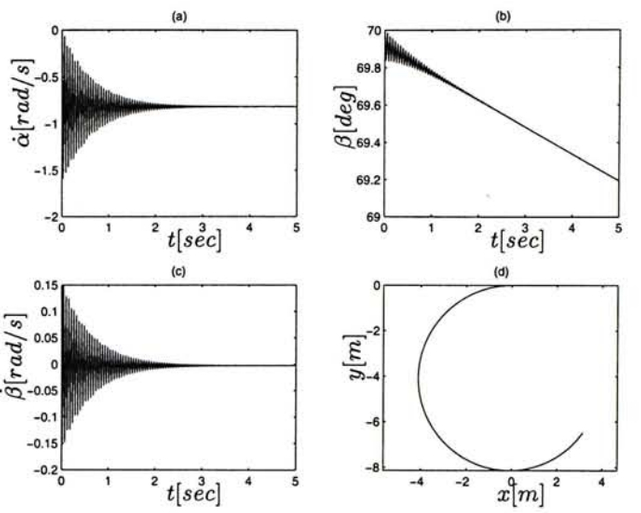

Figure 2.10: The simulation results of the single wheel robot.

and that of the single wheel robot, respectively, under the same initial conditions

$$\begin{cases} \beta = 70°, \beta_a = 0°, \\ \dot{\beta} = \dot{\alpha} = \dot{\beta}_a = 0\ rad/s, \dot{\gamma} = 15\ rad/s, \\ \alpha = 0°. \end{cases}$$

Note that the lean angle β of a rolling disk without the flywheel decreases more rapidly than that of the single wheel robot as shown in Figures 2.9b and 2.10b. This verifies the stabilizing effect of the flywheel on the single wheel robot. In Figures 2.10a-c, under the influence of friction in the yaw direction, the steering rate $\dot{\alpha}$ and the leaning rate $\dot{\beta}$ will converge to a steady state solution as shown in Eq. (2.50). Otherwise, the unwanted high frequency oscillation will occur. Practically, it will not produce a significant effect on the system because the frequency of the above oscillation is much greater than the system response. If the rolling speed of the disk is reduced, the rolling disk will fall much quickly.

Until now, we consider only the case when the flywheel's orientation is fixed with respect to the wheel. Here, we will focus on the tilting effect of the flywheel to the robot. Based on the conservation of angular momemtum, when the tilt angle of the flywheel β_a changes, the whole robot will rotate in the *opposite direction* in order to maintain a constant angular momentum. It implies that we may control the lean angle of the robot for steering. Simulation and experiment results are shown in Figure 2.11 and Figure 2.12, respectively,

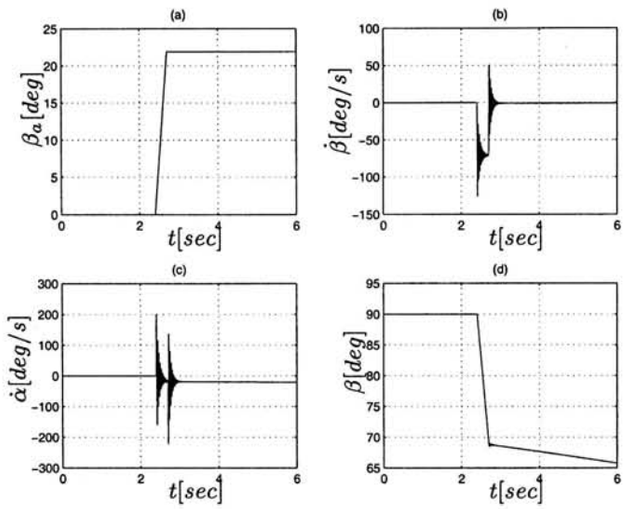

Figure 2.11: The simulation results of tilting the flywheel of the robot with $\dot{\beta}_a = 73\ deg/s$

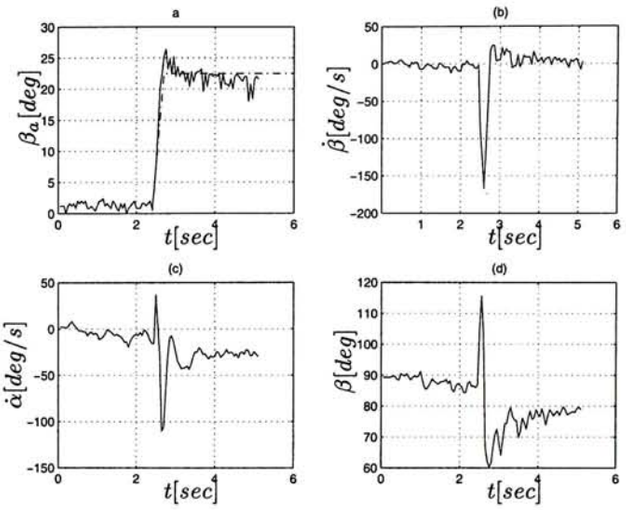

Figure 2.12: The experiment results of tilting the flywheel of the robot with $\dot{\beta}_a = 73\ deg/s$

under the same initial conditions

$$\begin{cases} \beta = 90°, \beta_a = \alpha = 0°, \\ \dot{\beta} = \dot{\alpha} = \dot{\beta}_a = 0\ rad/s, \dot{\gamma} = 15\ rad/s, \\ \alpha = 0°. \end{cases}$$

Both Figures 2.11 and 2.12 show that if the tilt angle β_a rotates in 73 deg/s counterclockwise at t = 2.4 second, the lean angle β rotates in clockwise direction . In the experiment, the transient response of β is more critical than the simulations. For 2.7 second, the tilt angle remains unchange and then the lean angle β and steering rate $\dot{\alpha}$ converge to steady state values in both simulations and experiments. In the experiment, we have not found any high frequency oscillations perhaps because the sensor response and the sampling time are much slower than the high frequency oscillations.

Chapter 3

Stabilization of the Single Wheel Robot

In the previous chapter, we investigated the kinematics and dynamics of the single wheel robot. In this chapter, We first linearize the dynamic model around the vertical position, and then study the controllability and the non-minimum phase behaviour of the robot. We propose a linear state feedback controller for stabilizing the robot to different lean angles, so as to control the steering velocity of the robot.

3.1 Linearized model

In Section 2.3, we showed that the model of the single wheel robot is highly coupled, nonholonomic and underactuated. In fact, the robot is inherently unstable in the lateral direction, the stabilization of the robot is always necessary. Moreover, owing to the absence of special steering mechanism such as a steering front wheel, the robot steers only by leaning itself to a predefined roll angle. In general, if the robot wants to steer to the left hand side, it leans toward the left hand side. Hence, the stabilization of the robot is important not only for balancing, but also for steering. The key problem for the stabilization of the robot is the coupling effect between the yaw and roll motions while no actuator can be used directly for the control of the roll motion.

There have been some work on the dynamics and control of autonomous unicycle and bicycle. Schoonwinkel [36] built an autonomous stabilized unicycle. He modeled the human-riding-unicycle system as a three-bodies system, i.e., a wheel, a frame and a rotary turntable. He separated the lateral and longitudinal dynamics by perturbating the yaw rate to specific quantities. Based on the model of Schoonwinkel, Vos and von Flotow [41] implemented the new LQG controller for the stabilization of the unicycle and dealt with the nonlinear problem of dry friction between the wheel and floor in the yaw direction. Both the unicycle of

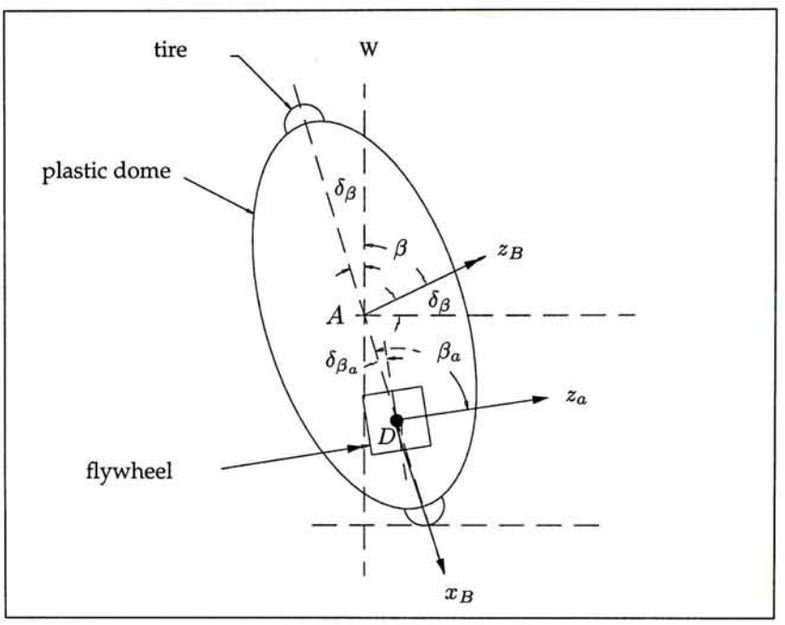

Figure 3.1: The lateral description of the linearized model.

Vos and Schoonwinkel used an actuator, reacting against the turntable to provide continuous yaw rate for the stabilization in the lateral motion. Sheng and Yamafuji [37] modeled the unicycle with a wheel, two closed link mechanisms and a rotary turntable. Nakajima et al. [26] designed an unicycle which is similar to a rugby ball where there is a rotary actuator between the upper and lower body. The unicycle can be stabilized by swinging the upper body. They also decoupled the lateral and longitudinal motions. It is different from our model because they did not consider the yaw dynamics and the coupling effect between the yaw and roll motions. Beznos et al. [5] studied a gyroscopically stabilized bicycle consisting of two coupled gyroscopes spinning in the opposite directions. They presented a linear model of the bicycle and a control law to track a straight line as well as a curve. However, the yaw dynamics was not taken into account and the steering angle of the front wheel was decoupled from the dynamics.

Most of the above mentioned work focus only on the stabilization of their robot to the upright position, but not any desired lean angle, except [26]. The single wheel robot steers by leaning to different roll angles. Therefore, it is necessary to design a controller that can stabilize the lean angle to any desired value, so as to control the steering velocity. Furthermore, we consider only the lateral stability of the single wheel robot because all its components are inside the wheel. However, for the unicycle type robot such as [36] and

Table 3.1: Variables definition for the linearized model

μ_s, μ_g	Friction coefficient in yaw and pitch directions respectively
Ω_o, Ω	Nominal component and the small perturbation of the wheel angular velocity respectively
δ_β	Small perturbation of the lean angle around vertical position
δ_{β_a}	Small perturbation of the tilt angle around vertical position

[41], its actuation mechanisms are built outside the wheel, both the lateral and longitudinal stability should be considered. The steering velocity of the single wheel robot is the same as the yaw rat $\dot{\alpha}$ because there is no special steering mechanism in our robot.

We derive a linear model based on the following assumptions: the spinning rate $\dot{\gamma}_a$ is sufficiently large so that the terms $\dot{\gamma}_a\dot{\beta}, \dot{\gamma}_a\dot{\alpha}$ are much larger than the terms $\dot{\beta}\dot{\gamma}, \dot{\beta}\dot{\alpha}, \dot{\alpha}^2$. We then linearize the system Eq. (2.48) around the vertical position with $\beta = 90^o + \delta_\beta, \dot{\gamma} = \Omega_o + \Omega, \beta_a = \delta_{\beta_a}$. The definition of variables and the configuration of the linearized model are shown in Table 3.1 and Figure 3.1 respectively. The lineared model is

$$\begin{aligned}
(I_{xf} + I_{xw})\ddot{\alpha} &= 2(I_{xw}\Omega_o + I_{xf}\dot{\gamma}_a)\dot{\delta}_\beta - \mu_s \\
&\quad +2I_{xf}\dot{\gamma}_a u_{\beta_a} \qquad (3.1) \\
(I_{xw} + mR^2)\ddot{\delta}_\beta &= gmR\delta_\beta - (2I_{xw} + mR^2)\Omega_o\dot{\alpha} \\
&\quad -2Ixf\dot{\gamma}_a\dot{\alpha} \qquad (3.2) \\
(2I_{xw} + mR^2)\dot{\Omega} &= -\mu_g\Omega + u_1 \qquad (3.3)
\end{aligned}$$

Because Ω is independent of the roll and yaw dynamics Eqs. (3.1) and (3.2), we can decompose the pitch dynamics Eq. (3.3) and setup a close loop for controlling the angular velocity of the robot Ω. The remaining yaw and roll dynamics form a state equation as,

$$\dot{x} = Ax + Gu, \qquad (3.4)$$

where $x = \left[\delta_\beta, \dot{\alpha}, \dot{\delta}_\beta\right]^T$,

$$A = \begin{bmatrix} 0 & 0 & 1 \\ 0 & a_{22} & a_{23} \\ a_{31} & a_{32} & 0 \end{bmatrix}, G = \begin{bmatrix} 0 \\ b_2 \\ 0 \end{bmatrix}$$

where $a_{22}, ..., a_{32}$ and b_2 are derived from Eqs. (3.1) and (3.2).

3.2 Controllability and non-minimum phase characteristics

Let $\mathcal{C}(A, B)$ be the controllability matrix of the system Eq. (3.4), then

$$\begin{aligned} |\mathcal{C}(A,B)| &= a_{32}^2 b_2^3 \\ &= \left(\frac{(2I_{xxw} + mR^2)\Omega_o + 2I_{xxf}\dot{\gamma}_a}{I_{xxw} + mR^2}\right)^2 \left(\frac{2I_{xxf}\dot{\gamma}_a}{I_{xxf} + I_{xxw}}\right)^3 \end{aligned} \tag{3.5}$$

From Eq. (3.5), the system is controllable if $\dot{\gamma}_a \neq 0$. It is because if the spinning rate of the flwheel is equal to zero, the flywheel does not provide an additional stabilizing force for balancing the robot.

To achieve the path following of the robot, it is desirable to control the forward speed and the steering velocity. From Eq. (3.3), we can control the forward speed by perturbating the nominal rolling speed (Ω_o) to any desired value. However, for the control of steering velocity, it exhibits non-minimum phase behaviour. If we consider the steering velocity $\dot{\alpha}$ as the output of Eq. (3.4). Then the transfer function will become

$$\begin{aligned} H(s) &= c(sI - A)^{-1} b \\ &= \frac{b_2(-a_{31} + s^2)}{s^3 - a_{22}s^2 - (a_{31} + a_{23}a_{32})s + a_{22}a_{31}} \end{aligned} \tag{3.6}$$

where $c = [0, 1, 0]$ and $b = G = [0, b_2, 0]^T$. Note that there is a zero of $H(s)$ on the right-half plane, therefore it is non-minimum phase. It means that the robot will fall if we control only the steering rate $\dot{\alpha}$ of the robot.

3.3 Linear state feedback

we propose a linear state feedback,

$$u_{\beta_a} = -k_1\delta_\beta - k_2\dot{\delta}_\beta - k_3\dot{\alpha}, \tag{3.7}$$

for stabilizing the system to an equilibrium (upright position) such that

$$\delta_\beta = 0, \quad \dot{\delta}_\beta = \dot{\alpha} = 0\ rad/s, \quad \ddot{\delta}_\beta = \ddot{\alpha} = \dot{\Omega} = 0\ rad/s^2$$

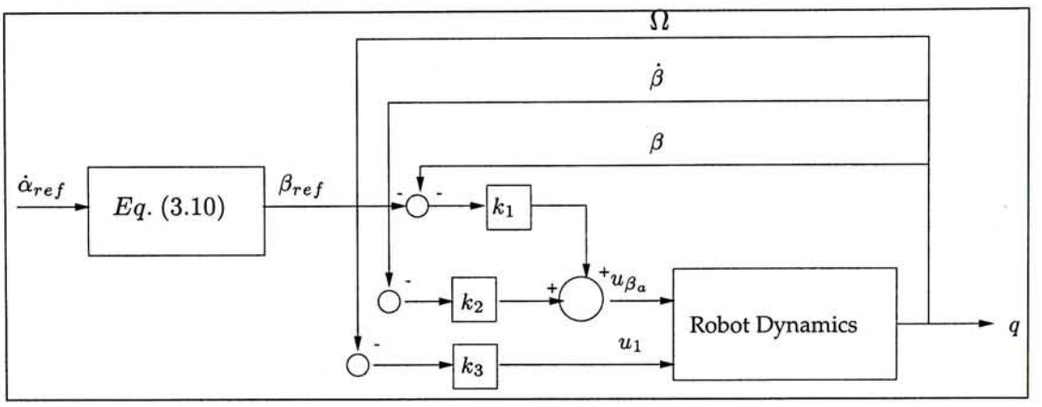

Figure 3.2: Schematic of the control algorithms.

where k_1, k_2, k_3 are feedback gains. In order to ensure an asymptotic stability of the system Eq. (3.4), the necessary conditions of the feedback gains are

$$k_1 < 0, k_2 < 0, k_3 > 0.$$

It ensures that all eignvalues of the closed loop system have negative real parts.

On the other hand, if we stabilize the system to a desired lean angle $\delta_{\beta ref}$ such that

$$\delta_\beta = \delta_{\beta ref}, \ \dot{\alpha} = \dot{\alpha}_s, \ \dot{\delta}_\beta = 0 \, rad/s, \ \ddot{\delta}_\beta = \ddot{\alpha} = \dot{\Omega} = 0 \, rad/s^2, \tag{3.8}$$

then the control law Eq. (3.7) will become

$$u_{\beta_a} = -k_1(\delta_\beta - \delta_{\beta ref}) - k_2\dot{\delta}_\beta - k_3(\dot{\alpha} - \dot{\alpha}_s). \tag{3.9}$$

where $\dot{\alpha}_s$ is the equilibrium steering rate under the conditions Eq. (3.8), that is

$$\dot{\alpha}_s = \frac{gmR\delta_{\beta ref}}{(2I_{xxw} + mR^2)\Omega_o + 2I_{xxf}\dot{\gamma}_a} \tag{3.10}$$

Given the nominal rolling speed Ω_o, the equilibrium steering rate $\dot{\alpha}_s$ is corresponding to one and only one lean angle $\delta_{\beta ref}$. Thus $\delta_{\beta ref}$ and $\dot{\alpha}_s$ can not be selected independently. This is the nonholonomic characteristics of the robot mentioned in Chapter 2.

We track a desired path by controlling the steering velocity $\dot{\alpha}$. However, the robot may fall if we only focus on the control of the steering velocity due to the non-minimum phase behaviour. In oder to track a desired steering velocity $\dot{\alpha}_{ref}$, we propose to track a roll angle $\delta_{\beta ref}$ that will be corresponding to the desired steering velocity based on Eq. (3.10). It is

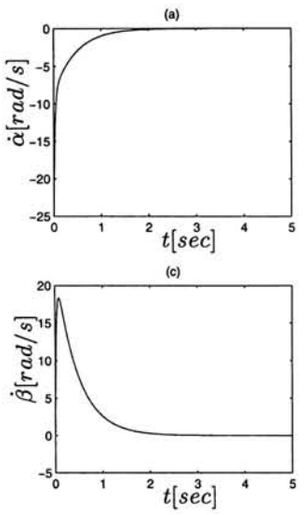

Figure 3.3: The simulation results of the single wheel robot stabilized to vertical position.

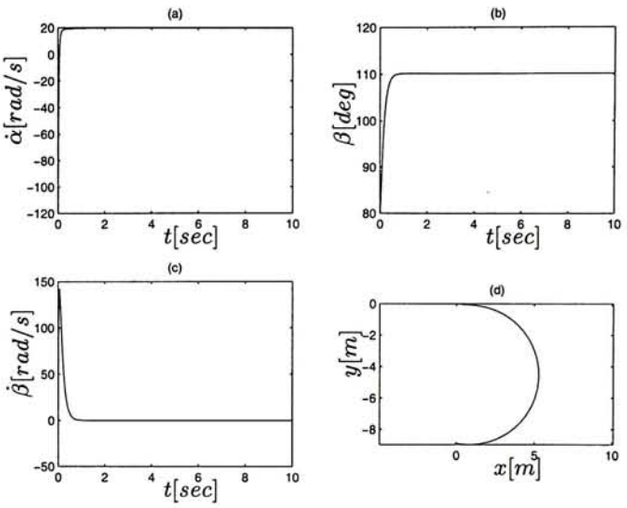

Figure 3.4: The simulation results of the single wheel robot stabilized to $\delta_{\beta ref} = 20°$.

because the equilibrium steering velocity $\dot{\alpha}_s$ of the roll angle $\delta_{\beta ref}$ is equal to the desired steering velocity $\dot{\alpha}_{ref}$. Then we setup a closed loop control for tracking the $\delta_{\beta ref}$ according to Eq. (3.9). The schematic diagram for the control of the steering rate is shown in Figure 3.2. Finally, we need setup a control loop for tracking the desired $\beta_a(t)$ to provide the suitable u_{β_a} for the closed loop system Eq. (3.4).

3.4 Simulation Study

First, we stabilize the robot to the upright position ($\beta = 90^o, \delta_{\beta ref} = 0^o$), such that the resulting trajectory is a straight line. The simulation results are shown in Figure 3.3. The initial conditions are,

$$\begin{cases} \delta_\beta = 10°, \beta_a = \alpha = 0°, \\ \dot{\delta}_\beta = \dot{\alpha} = \dot{\beta}_a = 0\ rad/s, \dot{\gamma} = 15\ rad/s, \\ k_1 = -15, k_2 = -1, k_3 = 3, \Omega_o = 15\ rad/s \end{cases}$$

From Figure 3.3, it shows that the lean angle β exponentially converge to 90°, so that the steering rate will exponentially converge to zero. Therefore the trajectory of the center of

the robot is slight curved at the beginning and then finally converges to a straight line.

Then we set $\delta_{\beta ref} = 20°$ and the simulation results are shown in Figure 3.4. Note that since $\delta_{\beta ref}$ is not eqaul to zero, there exits an equilibrium steering rate $\dot{\alpha}_s$ according to Eq. (3.10). Thus, the resulting trajectory is a circle.

Chapter 4

Path Following of the Single Wheel Robot

In this chapter, we first study the problem of the path following of vehicles with nonholonomic constraints, and then discuss the difficulty in controlling our robot for the path following. We describe the robot motion by a set of configurations using the path curvature and design a controller for the line following. The line following controller is divided into two parts: (1) velocity inputs are designed for the kinematic model to make the position and orientation error asymptotically stable. This is called the velocity control law. (2) torque control law is designed such that the linear and steering velocities of the robot converge to the velocities obtained from the velocity control law. We consider the derivative of the path curvature as the velocity control law. It is expressed as a linear combination of the current vehicle path curvature, heading angle and the position error. We demonstrate the asymptotic stability of the velocity control law. For torque control law, we use the linear state feedback to stabilize the robot to the desiged lean angle which is corresponding to the steering velocity obtained from the velocity control law. We investigate the effects of the initial heading angle, the rolling speed and the controller gains to the path following controller.

4.1 Path following for nonholonomic systems

In Section 2.1.1, we showed that the kinematic constraints of the single wheel robot are nonholonomic due to the rolling constraints. Many researches have been done in navigation problem [1] of a mobile robot under the nonholonomic velocity constraints (The first order nonholonomic constraints). Kolmanovsky and McClamroch [21] proposed the backstepping control approach that provides a rigorous method of taking into account the specific

[1]Navigation problem of a mobile robot normally divides into three basic problems: tracking a reference trajectory, following a path, and point stabilization.

vehicle dynamics to convert the kinematic model command into control inputs for the actual vehicle. First, feedback velocity control inputs are designed for the kinematic system to make the position error asymptotically stable. Then, a computed-torque controller is designed such that the mobile robots velocity converge to the given velocity inputs. Thus one can control kinemtic model and dynamic model separately as shown in [30] and [9]. Kanayama et al. [18] developed a stable control law to determine a vehicle's linear and rotational velocities, so as to follow a path while tracking the reference linear and rotational velocities. The stability of the rule was proved through the use of a Liapunov function. Samson [33] proposed a smooth time varying feedback laws for the path following of a chained system of wheeled robots. Canudas and Sordalen [39] also proposed a piecewise feedback laws for exponentially stabilizing a mobile robot. Rui [30] also proposed a control law for the path tracking of a rolling disk, which is not constrained to the vertical position, using the dynamic extension. However, in his model, he assumed that there is a torque directly acting on the roll direction of the disk for stabilization.

Most of them considered the kinematic constraints of the vehicles with steering front wheel as

$$\begin{bmatrix} \dot{x} \\ \dot{y} \\ \dot{\theta} \end{bmatrix} = \begin{bmatrix} C_\theta & 0 \\ S_\theta & 0 \\ 0 & 1 \end{bmatrix} \begin{bmatrix} v \\ \omega \end{bmatrix} \tag{4.1}$$

where (x, y) is the position of the center of the vehicles, θ is the orientation, and (v, ω) are the linear velocity and the rotational velocity respectively. The difficulty on solving the navigation problem of the vehicles under this constraints lies in fact that they have three degrees of freedom x, y and θ in its positioning but only two control inputs v, ω. In other words, just because the vehicle is nonholonomic. However, the constraints of the single wheel robot Eqs. (2.7) and (2.8) are different from the above constraints Eq. (4.1). There are drift terms introduced in Eqs. (2.7) and (2.8) because no actuator acts on the roll direction such that the terms coupled with the lean rate $\dot{\beta}$ become the drift terms. Therefore, the difficulty on solving the path following problem of the single wheel robot lies in fact that the vehicles not only control the position (x, y) and the orientation θ using two control input (v, ω), but also control the lean angle β within a stable region. If it fail, the robot falls.

Furthermore, the constraints Eq. (4.1) allow point steering of the front wheel. However,

for the single wheel robot, it is not allowed to have point steering while the derivative of path curvature must be continuous. Therefore, the above mentioned methods are not suitable to our robot. The purpose of this chapter is to present our proposed control algorithm for solving the path following problem of the single wheel robot which is nonholonomic and underactuated in roll dynamics.

4.2 Definition of path following

In this section, we define the path following problem of the vehicles and identify the differences between the trajectory tracking and the path following. The definition of the path following is:

> Given a path $P(s)$ in the plane, and the linear velocity of the vehicles $v(t)$, find a smooth (angular) velocity input $\mathbf{v}_c(t) = f_c(e_\theta, v, b, \mathbf{K})$ such that $\lim_{t\to\infty} e_\theta = 0$ and $\lim_{t\to\infty} b(t) = 0$, where e_θ, $b(t)$ and $\mathbf{K}$ are the the orientation error, the distance between a reference point in the vehicles and the path $P(s)$ and the controller gain vector, respectively. Then compute the torque τ for the dynamic model, such that $\mathbf{v} \to \mathbf{v}_c$ as $t \to \infty$.

The path following is different from the trajectory tracking. In the trajectory tracking, the desired time history of the output variables is specified. Therefore, in this case, the task is not only to reach a point, but also to reach a point at a specified time instant. However, in the path following, the desired path $P_d(s)$ is specified on the geometry of the path. In this case, the task is only to follow the path as closely as possible.

4.3 New configuration

In Section 4.1, we showed that the nonholonomic constraints of the robot are different from that of the typical mobile robot because it is perturbed from the vertical position. The constraints of the robot are

$$\dot{X}_c = R(\dot{\gamma}C_\alpha + \dot{\alpha}C_\alpha C_\beta - \dot{\beta}S_\alpha S_\beta) \tag{4.2}$$

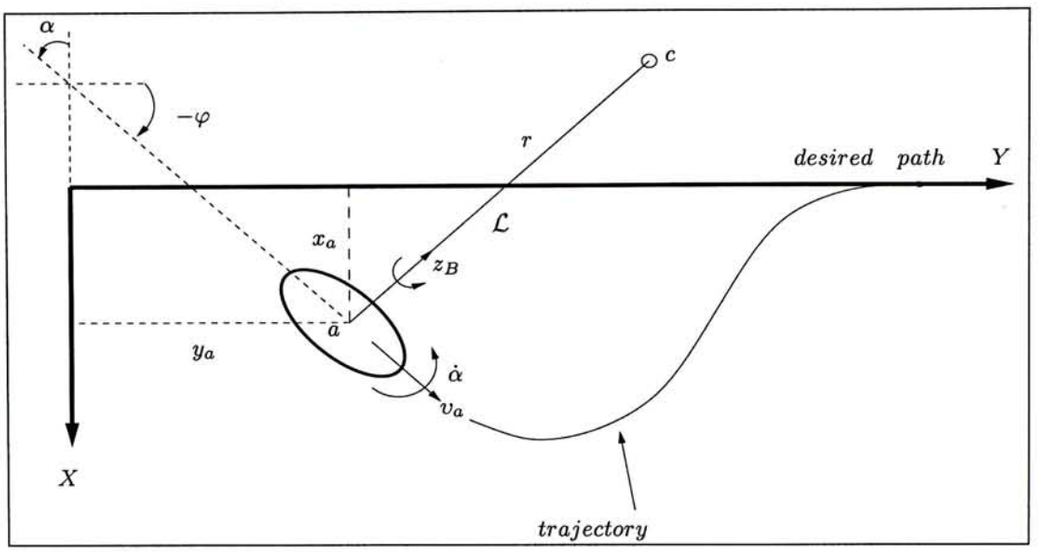

Figure 4.1: Principle of line following.

$$\dot{Y}_c = R(\dot{\gamma}S_\alpha + \dot{\alpha}C_\beta S_\alpha + \dot{\beta}C_\alpha S_\beta) \tag{4.3}$$

Note that the rolling speed $\dot{\gamma}$ and the yaw rate $\dot{\alpha}$ are the inputs to the system Eqs. (4.2) and (4.3), while the lean rate $\dot{\beta}$ can not be directly controlled because there is no external torque acting on the roll direction. It is hard to solve the navigation problem of this nonholonomic system with drift terms. In order to simplify the problem, we redefine the configuration of the robot based on the characteristics of the nonholonomic motion.

In the previous chapter, we normally considered the center of mass (X_c, Y_c) to be the position of the robot. However, for the path following, the robot need track a desired path on the ground, it is better to use the point of contact a on the ground to describe the position of the robot, instead of the center of mass.(Figure 2.6) Let (x_a, y_a) be the coordinates of the contact point a on this locus that coincides with a point of contact p of the robot. x_a and y_a can be expressed as

$$\begin{bmatrix} x_a \\ y_a \end{bmatrix} = \begin{bmatrix} X_c - RS_\alpha C_\beta \\ Y_c + RC_\alpha C_\beta \end{bmatrix} \tag{4.4}$$

Differentiate the Eq. (4.4) with respect to time, velocity constraints of the contact point a are,

$$\begin{bmatrix} \dot{x}_a \\ \dot{y}_a \end{bmatrix} = \begin{bmatrix} v_a C_\alpha \\ v_a S_\alpha \end{bmatrix} \tag{4.5}$$

where v_a is the contact point velocity,

$$v_a = R\dot{\gamma} \tag{4.6}$$

Note that Eq. (4.5) is independent of the lean angle β and is the same as the rolling constraints of a typical mobile robot, i.e. there is no drift term in Eq. (4.5).

The status of the contact point of the robot can be described by an alternative set of configurations based on [15],

$$q = (p, \varphi, \kappa) = ((x_a, y_a), \varphi, \kappa)\,, \tag{4.7}$$

where p, φ and κ are the position, heading orientation and the path curvature of the robot with respect to the inertial frame, respectively. The new configuration of the robot is shown in Figure 4.1. The heading orientation φ is measured about the X-axis while the yaw angle α is measured about the Y-axis. Then

$$\varphi = \alpha - \frac{\pi}{2}, \;\; \dot{\varphi} = \dot{\alpha}. \tag{4.8}$$

We include the path curvature in the new configuration, partially because a vehicle under the nonholonomic constraints can execute only a path that has curvature continuity [17].

The contact point a of the robot have three degrees of freedom x_a, y_a, φ but we only have two control inputs the steering velocity $\dot{\alpha}$ and the linear velocity v_a for this nonholonomic system. We can replace the original control inputs by the path curvature κ and the contact point velocity v_a because the motion of the contact point a undergoes nonholonomic motion [15]. Its path curvature κ can be expressed as,

$$\kappa(t) = \frac{d\varphi(t)}{ds} = \frac{\dot{\varphi}(t)}{v_a(t)} = \frac{\dot{\alpha}(t)}{v_a(t)} = \frac{1}{r(t)} \tag{4.9}$$

where $r(t)$, s and $\dot{\varphi}(t)$ are the radius of the curvature from the center of rotation c to the contact point a, the path length, and the rotational velocity of the robot, respectively.(Figure 4.1) If the center c of the rotation is at infinity, the robot is moving on a straight line and the path curvature and steering velocity are equal to zero.

4.4 Line following

For simplicity, we can decompose any path into straight lines and circular arcs. We design controllers for line tracking and circle tracking separately, and then make the robot follow

any paths consisting of lines and arcs by switching the path tracking controllers for the straight lines and circles as in [32]. At the first step, we need design a line following controller for the robot, so as to the circle one.

We divide the line following controller into two parts: (1) velocity inputs are designed for the kinematic model to make the position and orientation error asymptotically stable. This is called velocity control law. (2) torque control law is designed such that the linear and steering velocities of the robot converge to the designed velocities obtained from the velocity control law.

4.4.1 Velocity control law

Based on [15], we first design a control law to track the Y-axis and then extend to track any desired line. Traditionally, in order to achieve line following of a mobile robot, one designs feedback velocity inputs to control the kinematic model. However, we consider the path curvature as the feedback of the system, instead of the linear and steering velocities. It is because the robot can execute only a path with continuous path curvature due to the nonholonomic constraints. The path curvature is implicitly related with the constraints. It is a better variable to describe the motion control of the robot with nonholonomic constraints. For example, when we drive the automobile, we positively control the path curvature to follow the road through the steering front wheel. Therefore, we consider the derivative of the path curvature as the velocity control law and then express the derivative of the path curvature ($\frac{d\kappa}{ds}$) with respect to the path length s as :

$$\frac{d\kappa}{ds} = -a\kappa - b\varphi - cx_a, \tag{4.10}$$

where a, b and c are positive constants and Eq. (4.10) is called a steering function in [15]. If (a, b, c) are selected such that Eq. (4.10) is asymptotically stable, the continuity of the path curvature can be ensured and $\frac{d\kappa}{ds} \to 0$ as the path length s increases, i. e., $x_a \to 0$, $\kappa \to 0$ and $\varphi \to 0$ as s increases. Hence, the robot converges to the Y-axis asymptotically. The path curvative feedback κ can be found out by integrating the Eq. (4.10) in each instant. Given the linear velocity and the path curvature feedback, we can obtain the corresponding steering velocities $\dot{\alpha}$ for the robot according to Eq. (4.9).

4.4.2 Convergence for the velocity control law

To achieve convergence of the control law Eq. (4.10), we must select a proper set of (a, b, c). We introduce a new time scale which is identical to the distance along the desired path y_a and represent all the variables in Eq. (4.10) (x_a, φ, κ and $\frac{d\kappa}{ds}$) in terms of the derivative of x_a with respect to y_a. ($\frac{d^n x_a}{dy_a^n}$)

$$\varphi = tan^{-1}(\frac{dx_a}{dy_a}) \tag{4.11}$$

$$\begin{aligned} \kappa &= \frac{d\varphi}{ds} = \frac{\frac{d\varphi}{dy_a}}{\frac{ds}{dy_a}} \\ &= \frac{\frac{d^2x_a}{dy_a^2}}{(1+(\frac{dx_a}{y_a})^2)^{\frac{3}{2}}} \end{aligned} \tag{4.12}$$

$$\begin{aligned} \frac{d\kappa}{ds} &= \frac{\frac{d\kappa}{dy_a}}{\frac{ds}{dy_a}}, \\ &= \frac{d^3x_a}{dy_a^3}(1+\frac{dx_a}{dy_a}^2)^{-2} - 3\frac{dx_a}{dy_a}\frac{d^2x_a}{dy_a^2}\,{}^2(1+\frac{dx_a}{dy_a}^2)^{-3} \end{aligned} \tag{4.13}$$

Note that if $x_a \to 0$, $\frac{dx_a}{dy_a} \to 0$, $\frac{d^2x_a}{dy_a^2} \to 0$ and $\frac{d^3x_a}{dy_a^3} \to 0$, then $\varphi \to 0$, $\kappa \to 0$ and $\frac{d\kappa}{ds} \to 0$. Hence, the robot converges to the Y-axis. In order to track the Y-axis, x_a and its derivative with respect to y_a must converge to zero. To this end, we define a system of first order equation,

$$\frac{d\xi}{dy_a} = f(\xi), \tag{4.14}$$

where

$$\xi \equiv \begin{bmatrix} \xi_1 \\ \xi_2 \\ \xi_3 \end{bmatrix} \equiv \begin{bmatrix} x_a \\ \frac{dx_a}{dy_a} \\ \frac{d^2x_a}{dy_a^2} \end{bmatrix} \tag{4.15}$$

If the system Eq. (4.14) is asymptotically stable, the robot converges to the Y-axis from any initial configurations because x_a and its derivative with respect to y_a converge to zero asymptotically. After substituting Eqs. (4.10), (4.11), (4.12), and (4.13) into Eq. (4.14), we have

$$\frac{d\xi_1}{dy_a} = \frac{dx_a}{dy_a} = \xi_2, \tag{4.16}$$

$$\frac{d\xi_2}{dy_a} = \frac{d^2x_a}{dy_a^2} = \xi_3, \tag{4.17}$$

$$\begin{aligned}\frac{d\xi_3}{dy_a} &= \frac{d^3x_a}{dy_a^3} \\ &= 3\xi_2\xi_3^2(1+\xi_2^2)^{-1} - a\xi_3(1+\xi_2^2)^{\frac{1}{2}} \\ &\quad -b(1+\xi_2^2)^2 tan^{-1}\xi_2 - c\xi_1(1+\xi_2^2)^2\end{aligned} \tag{4.18}$$

Now we should choose a proper set of (a, b, c) such that the zero equilibrium of the system Eq. (4.14) is asymptotically stable. Using the Jacobian linearization, the system Eq. (4.14) become,

$$\frac{d\xi}{dy_a} = A\xi, \tag{4.19}$$

where

$$A = \left[\frac{df}{d\xi}\right]_{\xi=0} = \begin{bmatrix} 0 & 1 & 0 \\ 0 & 0 & 1 \\ -c & -b & -a \end{bmatrix} \tag{4.20}$$

To ensure the asymptotic stability of the system Eq. (4.19), all eigenvalues of A should have negative real parts. The characteristic equation of A is

$$\lambda^3 + a\lambda^2 + b\lambda + c = 0, \tag{4.21}$$

where λ are the eigenvalues of A. By Routh Hurwitz criterion, a, b and c must be larger than zero while $ab > c$. If all eigenvalues of A are equal to $-k$, then

$$a = 3k, \quad b = 3k^2, \quad c = k^3. \tag{4.22}$$

where k is the gain of the velocity control law. Based on Eq. (4.22), we can ensure the local convergence of the system Eq. (4.14) and the control law Eq. (4.10), such that the robot can converge to the Y-axis asymptotically. In [15], authors let

$$\sigma = \frac{1}{k} \tag{4.23}$$

where σ is called the smoothness of the velocity control law.

The global stability of the system can be proved using the following Lyapunov function:

$$V = \frac{b}{2c}\kappa^2 + \frac{b^2}{2c}\varphi^2 + \frac{c}{2}y_a^2 + by_a\varphi + \kappa S_\varphi + a(1 - C_\varphi), \tag{4.24}$$

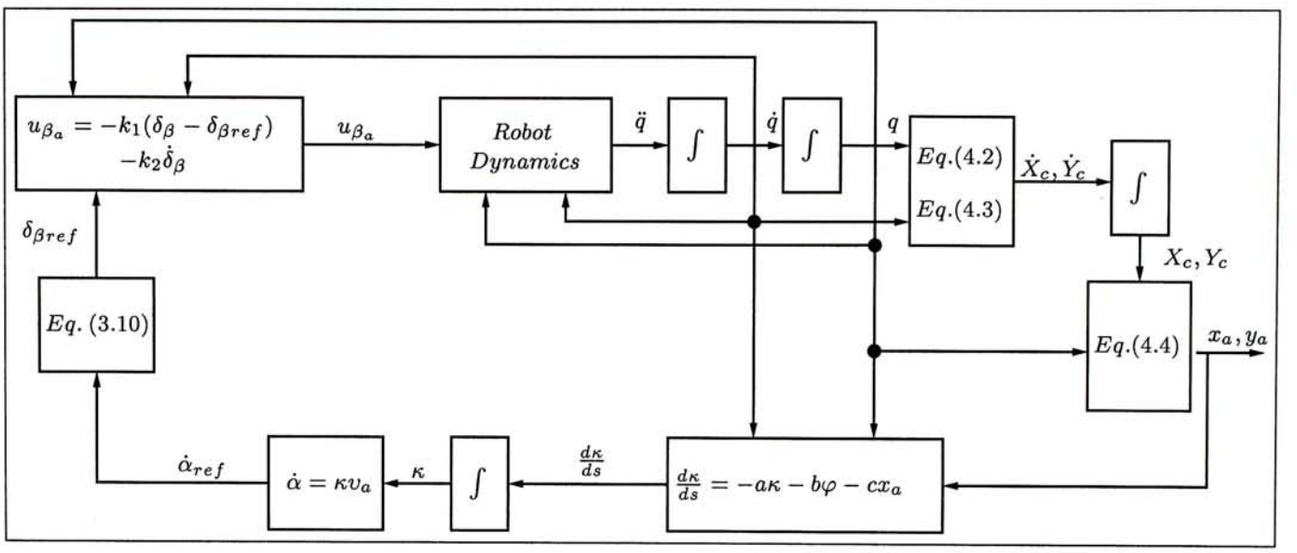

Figure 4.2: Schematic of the control algorithm for the Y-axis.

where a, b, c are positive constants in Eq. (4.10). The detailed prove of the global stability has been shown in [15].

4.4.3 Torque control law

In this section, we design the torque control such that the robot can track the path curvature obtained from integration of Eq. (4.10). Given the linear velocity of the robot, it can track the previously mentioned path curvature if its steering velocity $\dot{\alpha}$ converges to the corresponding values obtained from Eq. (4.9). The torque control problem reduces to design the torque inputs of the robot such that its path curvature converges to the desired value by controlling the steering velocity.

However, if we ignore the lateral stability during the path following, the robot falls down. In Section 3.3, we proposed an algorithm to control the steering velocity by tracking a lean angle trajectory $\delta_\beta(t)$ that is corresponding to the desired steering velocity $\dot{\alpha}_{ref}$ based on Eq. (3.10). Assuming that we can control the lean angle β faster than the control of the path curvature κ, we can consider κ to be fixed in the β time scale. The linear state feedback for stabilizing the robot to the desired lean angle is

$$u_{\beta_a} = -k_1(\delta_\beta - \delta_{\beta ref}(t)) - k_2\dot{\delta}_\beta \tag{4.25}$$

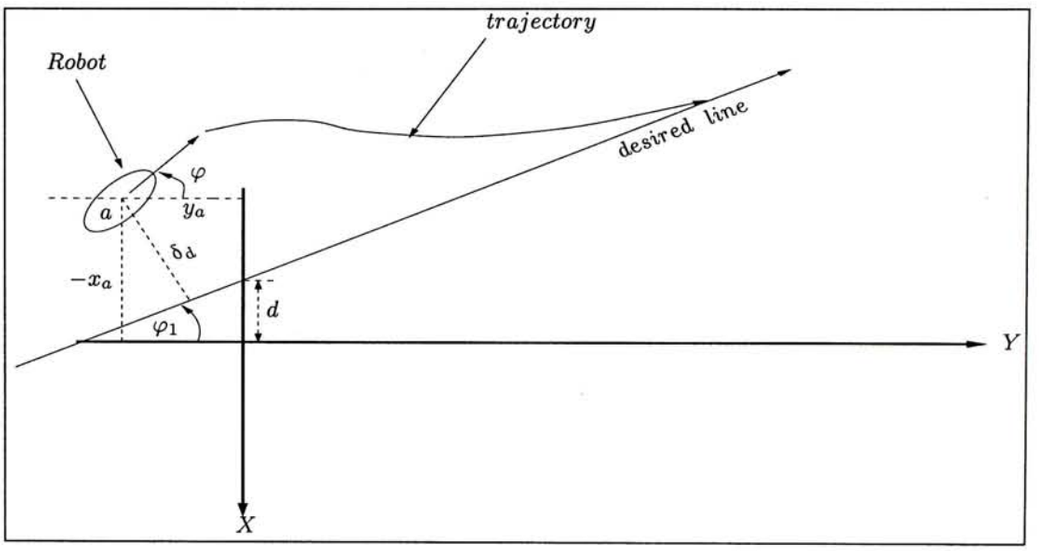

Figure 4.3: Following a desired line.

where δ_β and $\delta_{\beta ref}$ are the small pertubation of the lean angle from the vertical position and the reference lean angle respectively. Note that the steering velocity $\dot{\alpha}$ does not appear in Eq. (4.25) because if the robot stabilizes to the desired lean angle $\delta_{\beta ref}$, its steering rate must converge to an equilibrium value according to Eq. (3.10). Therefore, no need to include the steering velocity in the state feedback Eq. (4.25). The overall artichecture of the control algorithm has shown in Figure 4.2.

Remark: The Line following controller for the Y-axis can be extended to track any desired line by adjusting the derivative of the path curvature to the form as:

$$\frac{d\kappa}{ds} = -a\kappa - b(\varphi - \varphi_1) - c\delta_d, \tag{4.26}$$

where φ_1 and δ_d are the direction of the desired line and the perpendicular distance between the robot and the line respectively (Figure 4.3). Let the desired line be described by $Ax + By + C = 0$, then

$$\varphi_1 = \arctan\frac{B}{A}, \quad \delta_d = \frac{Ax_a + By_a + C}{\sqrt{A^2 + B^2}}. \tag{4.27}$$

where A, B, and C are constants. If $\delta_d > 0$, the robot is on the left side of the desired line and vice versa. If $\delta_d = 0$, the robot is on the line.

If we transform the original system by the tranformation matrix

$$T = \begin{bmatrix} C_{\varphi_1} & S_{\varphi_1} & 0 \\ -S_{\varphi_1} & C_{\varphi_1} & d \\ 0 & 0 & 1 \end{bmatrix}, \tag{4.28}$$

such that the desired line becomes the Y-axis of the global coordinates system. Then

$$\varphi_1 = 0, \delta_d = -x_a,$$

so that the prove of convergence for following any desired line is the same as the line following for the Y-axis.

4.5 Simulation study

4.5.1 Effect of the initial heading angle

In this section, we show three simulation results ($S1$, $S2$ and $S3$), in which the robot tracks the Y-axis, under different initial conditions. The simulation results and the initial conditions are shown in Figures 4.4, 4.5, 4.6 and Table 4.1, respectively. Within these three simulations, we control the rolling speed $\dot{\gamma}$ of the robot to a constant value (30 rad/s), by setting the nominal rolling speed Ω_o to this value, thus the contact point velocity v_a will also be constant. The smoothness sets to 30.

For simulation $S1$, the robot has smaller path curvature than in simulation $S2$ because its initial heading angle $\varphi(0)$ in simulation $S1$ is less deviated from the Y-axis than that of simualtion $S2$. Furthermore, since the robot has larger path curvature in simulation $S2$, the robot make sharper turns. To this end, the robot have to lean steeper for providing sufficient steering velocity $\dot{\alpha}$ than the case in simulation $S1$. This situation becomes more seriously in simulation $S3$. From Figure 4.6, it shows that the lean angle β becomes saturated before 5 sec. It is because the initial heading angle $\varphi(0)$ is more than $90°$, in order to ensure the curvature continuity while following the Y-axis, it should have largest path curvature among three such that the lean angle β of the robot is the steepest, so that it provides enough steering velocity. As we have already set up a limit for the state feedback controller, the lean angle can only be stabilized within $\beta \in (-60°, 60°)$, otherwise the controller will become

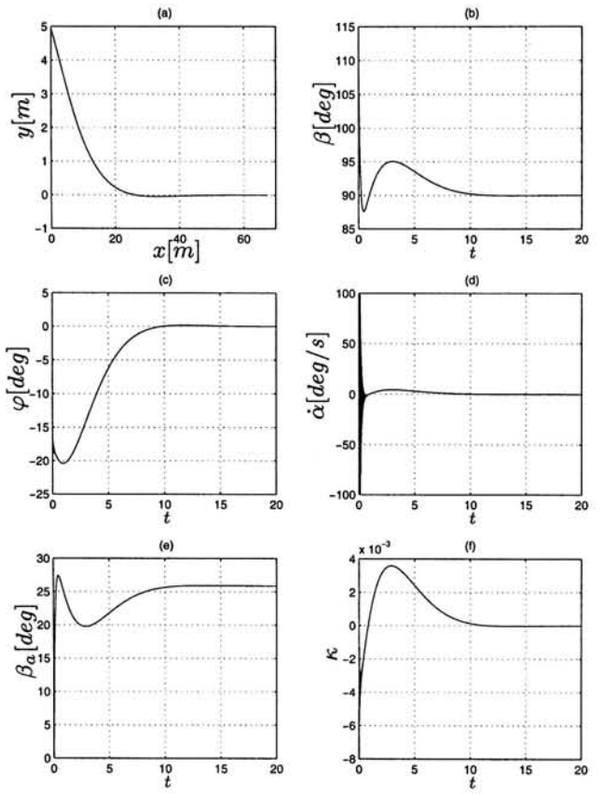

Figure 4.4: The simulation results ($S1$) for following the Y-axis.

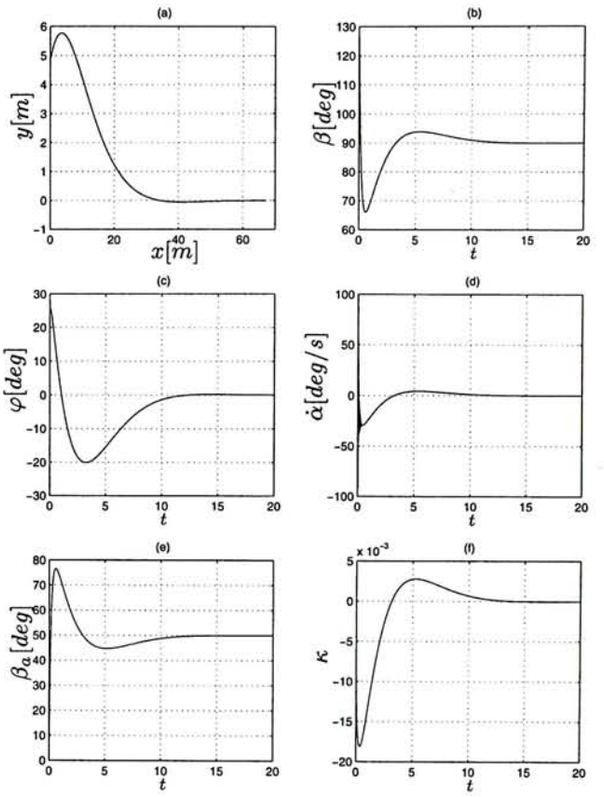

Figure 4.5: The simulation results ($S2$) for following the Y-axis.

saturated and lean angle will be fixed at the limiting value. When the robot gradually approaches to the Y-axis, the path curvature decreases so that the robot need not make sharp turns. Therefore, the lean angle gradually increase until it reaches to the vertical position. (90°)

Table 4.1: The initial conditions for the simulations $S1$, $S2$ and $S3$.

Simulation	X_a	Y_a	$\alpha(0)$	$\beta(0)$	$\gamma(0)$	$\dot{\alpha}(0)$	$\dot{\beta}(0)$	$\dot{\gamma}(0)$	$\kappa(0)$	$\beta_a(0)$	$\varphi(0)$
$S1$	$5[m]$	0	70°	110°	0	0	0	30 rad/s	0	0	$-20°$
$S2$	$5[m]$	0	110°	130°	0	0	0	30 rad/s	0	0	20°
$S3$	$5[m]$	0	210°	110°	0	0	0	30 rad/s	0	0	120°

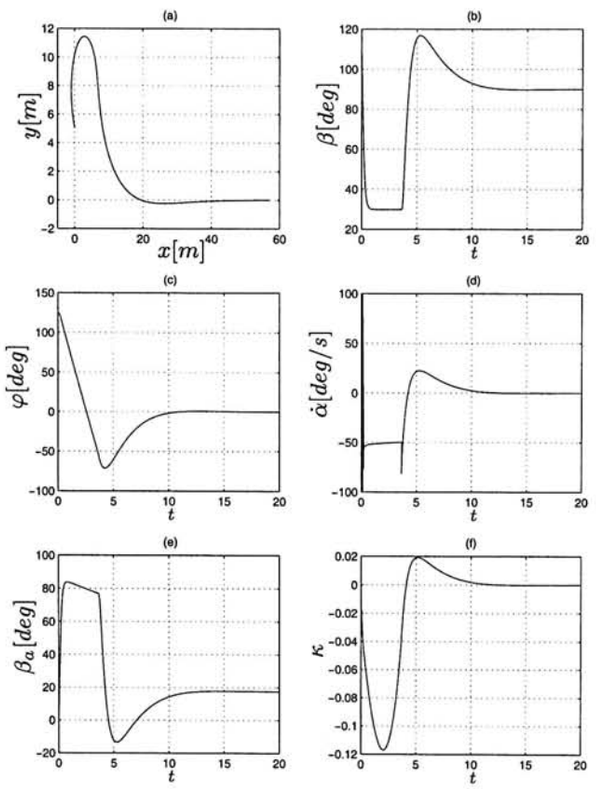

Figure 4.6: The simulation results ($S3$) of the robot for following the Y-axis.

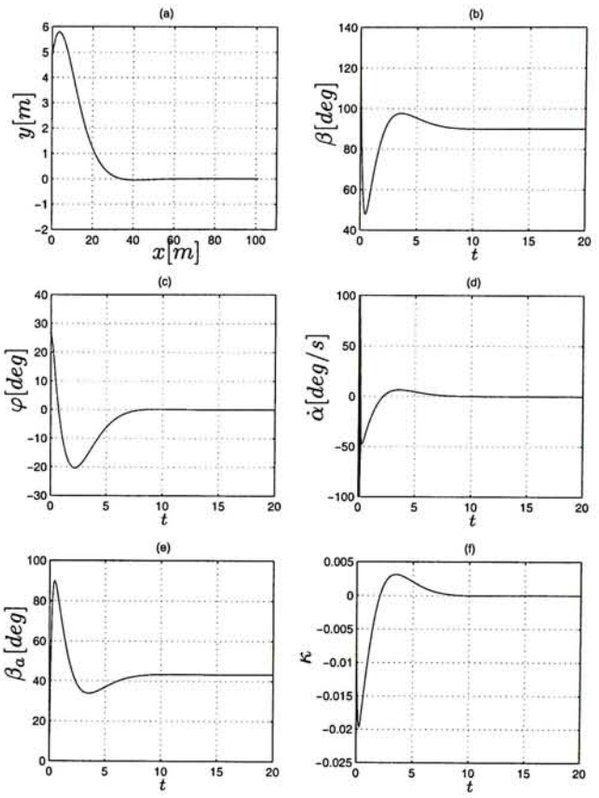

Figure 4.7: The simulation results for following the Y-axis with $\dot{\gamma} = 10 \ rad/s$.

4.5.2 Effect of the rolling speed

In this section, we study the effect of the rolling speed of the robot $\dot{\gamma}$ to the path following controller. The simulation results with different rolling speeds are shown in Figure 4.7 and 4.8. Both of them have the same initial conditions as in simulation $S1$. For $\dot{\gamma} = 30 \ rad/s$, the robot will converge to the Y-axis rapidly than the other one, comparing with Figure 4.7a and 4.8a. From Figure 4.7b and 4.8b, the change of the lean angle β of the robot with lower rolling speed is more significant than that of the robot with higher rolling speed. It is because if the robot has greater rolling speed, according to Eq. (4.9), less steering velocity is required for tracking the same path curvature feedback κ. Thus, the change of the lean angle β decreases based on Eq. (3.10).

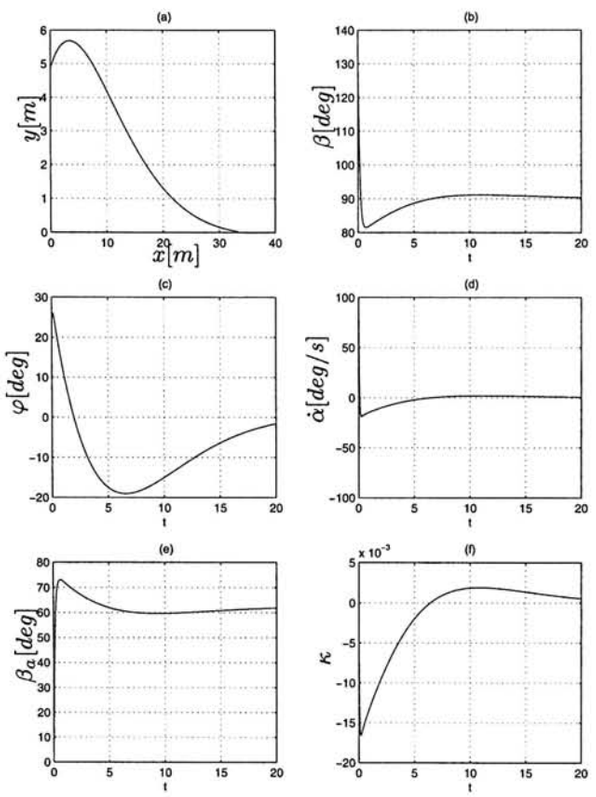

Figure 4.8: The simulation results for following the Y-axis with $\dot{\gamma} = 30\ rad/s$.

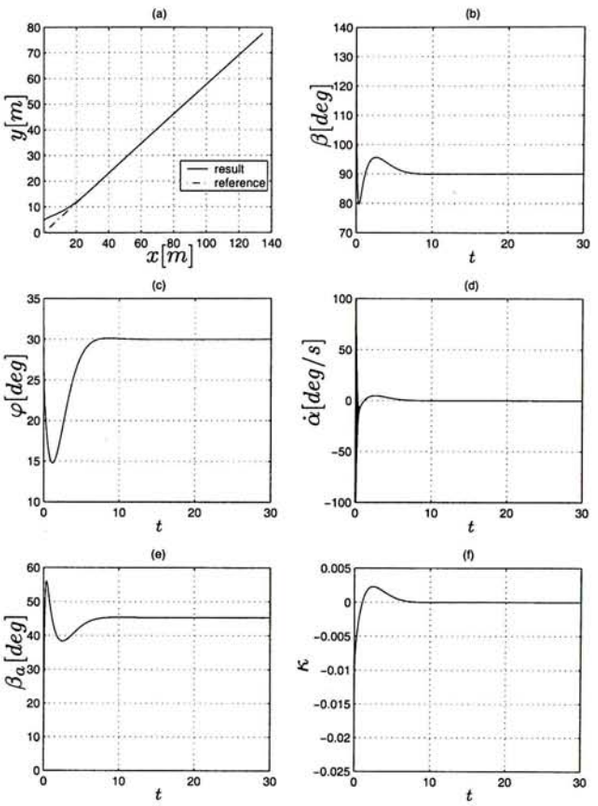

Figure 4.9: The simulation results for following a desired line $y = \tan 30° x$.

4.5.3 Follow a desired line

In this section, we show the simulation results of the robot to follow a desired line $y = \tan 30° x$. The simulation results are shown in Figure 4.9. The initial conditions in this simulation are identical to simulation $S1$. From Eq. (4.27),

$$\varphi_1 = \frac{\pi}{6}, \quad \delta_d = \frac{x_a - \tan 30° y_a}{\sec 30°}. \tag{4.29}$$

From Figure 4.9, the robot can follow the desired line while the lean angle β is not over the limiting value.

4.5.4 Effect of the smoothness parameter

In this section, we show the effect of the smoothness σ to the resulting path curvature of the robot. In [15], authors showed that a larger smoothness will have a smoother motion such

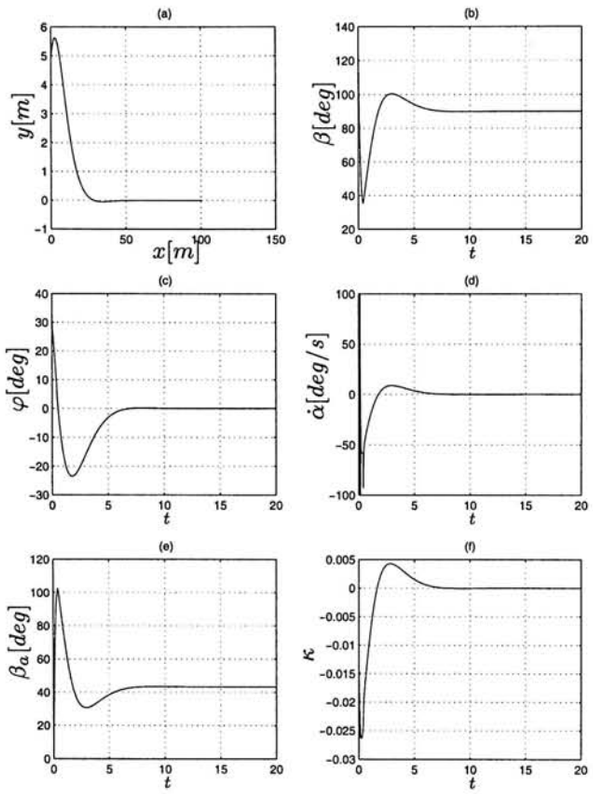

Figure 4.10: The simulation results for following the Y-axis with $\sigma = 20$.

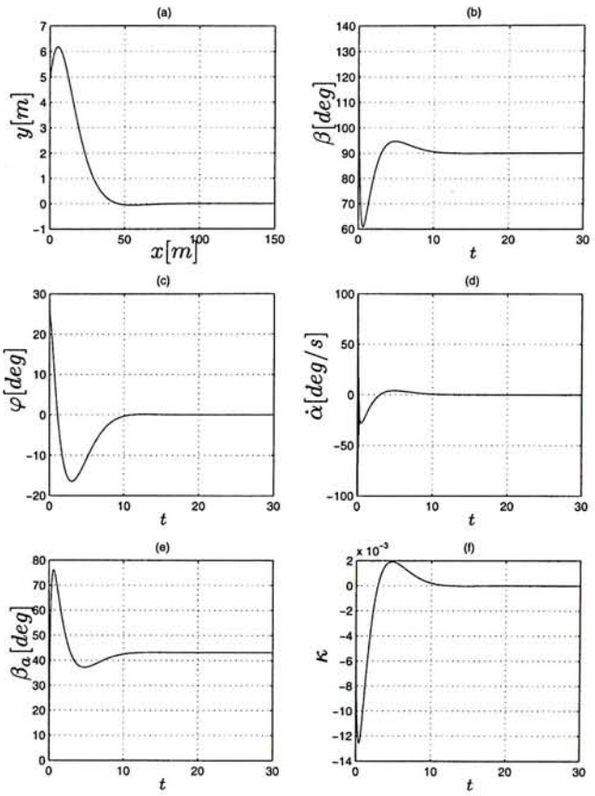

Figure 4.11: The simulation results for following the Y-axis with $\sigma = 40$.

that the resulting path curvature κ will be smaller. For the robot with smaller smoothness, the resulting path curvature will be larger, thus it converges to the desired line more quickly. Therefore, the smoothness not only affects the path curvature of the robot, but also affects the time spent / distance travelled the line following. The simulation results with different smoothnesses are shown in Figure 4.10 and 4.11 respectively. In Figure 4.10a, the robot converges to the Y-axis much rapidly than the case in Figure 4.11a. Therefore, for the robot with smaller smoothness, it will have larger path curvature and the change of lean angle than the robot with larger smoothness ratio. (Figure 4.10b,f and 4.11b,f)

Chapter 5
Conclusion

5.1 Contributions

In this thesis, we present a study of the fundamental characteristics of the single wheel robot, and develop a dynamic model and control methods of this robot. The original contributions of this thesis are summarized below.

- **Modeling.** We developed the kinametic and dynamic models of the single wheel robot. In derivation of the model, we consider the robot as a combination of three components: a rolling disk, an internal mechanism and a flywheel. They are linked by a two-link manipulator. We simplified the model by decoupled the tilt angle of the flywheel from the dynamics. We verified the model by experiment and simulation. We demonstrated that the dynamics of the robot is nonholonomic and underactuated. We demonstrated the dynamics coupling between the wheel and the flywheel, through the stabilization and tilting effect of the flywheel to the robot.

- **Stabilization.** We linearized the developed model by perturbating the rolling speed to specific quantities. The pitch angle is decoupled from the yaw and roll dynamics after linearization. We demonstrated the controllability and non-minimum phase behaviour of the model. We designed a linear state feedback for stabilizing the robot to any desired lean angle.

- **Path following.** We developed a controller for the single wheel robot to track any desired line. We divided the controller into two parts: (1) velocity inputs are designed for the kinematic model to ensure the position and orientation error to be asymptotically stable. This is called the velocity control law. (2) torque control law is designed

such that the linear and steering velocities converge to the desired velocities obtained from the velocity control law. In the first part, we considered the derivative of the path curvature as the velocity control law. We demonstrated the asymptotic stability of this control law. In the second part, we considered the linear state feedback as the torque control law. It is to stabilize the robot to the desired lean angle which is corresponding to the steering velocity obtained from the velocity control law. We investigated the effects of the initial heading angle, rolling speed and controller gains to the line following controller.

5.2 Future work

In this thesis, we provide the foundations of the dynamics and control of the single wheel robot. It is only the first step toward the automatic control of the robot. The following are possible improvements and extensions of this work:

- **Stabilization of the robot using nonlinear methods.** The linearized model simplifies the stabilization problem of the robot. However, the proposed linear state feedback only gurantees the local stability of the system. We desire to seek a nonlinear control methods for the stabilization such that the global stability of the system can be ensured. The nonlinear model of the robot is different from the ordinary underactuated systems such as the underactuated manipulators because this model does not have the off-diagonal terms in its inertia matrix, thus the roll dynamics of the robot is only velocity coupling between the yaw and pitch motions. Therefore, the typical nonlinear control methods for the underactuated manipulators are not suitable to the single wheel robot. One of the suggestions is the backstepping control method. If we assume that the rolling speed of the robot is fixed, the remaining system can be viewed as a cascade connection between the yaw and roll motions. The coupling of the two subsystems is through the steering velocity $\dot{\alpha}$ and the leaninf rate $\dot{\beta}$. This will become the standard form for applying the backstepping control method.

- **Circle following controller.** The proposed line following controller can be extended to the circle following. The basic idea for this controller can be adopted from [16]. In the

circle following controller, the reference path curvature is not fixed to zero and the reference heading angle is time-varying. After developing the circle following controller, we control the robot to track any paths consisting of lines and arcs by switching the path tracking controllers for the straight lines and circles.

- **Experiments.** Until now, we have not implemented the proposed linear state feedback and the line following controller to the single wheel robot. The robot have installed the gyros and tilt sensor to measure the angular velocities and lean angle respectively. It is possible to implement the proposed linear state feedback to stabilize the robot to any desired lean angle. For the line following controller, it is necessary to localize the position of the robot in real time before implemention of the line following controller. One of the suggestions is to use a CCD camera mounted on the ceiling to measure the position of the robot in real time.

Bibliography

[1] H. Arai and S. Tachi, "Position control of a manipulator with passive joints using dynamic coupling," *IEEE Trans. on Robotics and Automation*, vol. 8, no. 4, pp. 528-34, 1991.

[2] M. G. Bekker, *Theory of land locomotion*, University of Michigan Press, pp. 213-217, 1956.

[3] M. G. Bekker, "Accomplishments and future tasks in off-road transportation," *Journal of Terramechanics*, vol. 11, no. 2, pp. 11-30, Permagon Press, Ltd., 1974.

[4] M. Bergerman, C. Lee and Y. Xu, "A dynamic coupling index for underactuated manipulators," *Journal of Robotic Systems*, vol. 12, no. 10, pp. 693-707, 1995.

[5] A. V. Beznos, et. al., "Control of autonomous motion of two-wheel bicycle with gyroscopic stabilisation," *Proc. IEEE Int. Conf. on Robotics and Automation*, vol. 3, pp. 2670-75, 1998.

[6] A. M. Bloch, M. Reyhanoglu and N. H. McClamroch, "Control and stabilization of nonholonomic systems," *IEEE Trans. on Aut. Control*, vol. 37, pp. 1746-1757, 1992.

[7] H. B. Brown and Y. Xu, "A single wheel gyroscopically stabilized robot." *Proc. IEEE Int. Conf. on Robotics and Automation*, vol. 4, pp. 3658-63, 1996.

[8] S. Dubowsky and E. Papadopoulos, "The kinematics, dynamics and control of the free-flying and free-floating space robotic systems," *IEEE Trans. on Robotics and Automation*, vol 9, no. 5, pp. 531-43, 1993.

[9] R. Fierro and F. L. Lewis "Control of a nonholonomic mobile robot: Backstepping kinematics into dynamics," *Journal of Robotic Systems*, vol. 14, no. 13, pp. 149-163, 1997.

[10] D. R. Freitag, "History of wheels for off-road transport," *Journal of Terramechanics*, vol. 16, no. 2, pp. 49-68 , Permagon Press, Ltd., 1979.

[11] N. H. Getz, "Control of balance for a nonlinear nonholonomic non-minimum phase model of a bicycle," *Proc. ACC*, vol. 1, pp. 148-151.

[12] N. H. Getz and J. E. Marsden "Control of an autonomous bicycle," *Proc. IEEE Int. Conf. on Robotics and Automation*, vol. 3, pp. 1397-1402, 1995.

[13] J. Hauser and R. M. Murray "Nonlinear controllers for non-integrable systems: the Acrobot example," *Proc. ACC*, vol. 1, pp. 669-71, 1990.

[14] I. C. Holm, "Articulated, wheeled off-road vehicles," *Journal of Terramechanics*, vol. 7, no. 1, pp. 19-54, Permagon Press, Ltd., 1970.

[15] Y. J. Kanayama and F. Fahroo, "A new line tracking method for nonholonomic vehicles," *Proc. IEEE Int. Conf. on Robotics and Automation*, vol. 4, pp. 2908-11, 1997.

[16] Y. J. Kanayama and F. Fahroo, "A circle tracking method for nonholonomic vehicles," *The Fifth IFAC Symp. on Robot Control*, vol. 2, pp. 551-558, 1997.

[17] Y. J. Kanayama, "Two dimensional wheeled vehicle kinematics," *Proc. IEEE Int. Conf. on Robotics and Automation*, vol. 4, pp. 3079-84, 1994.

[18] Y. J. Kanayama, Y. Kimura, F. Miyazaki, and T. Noguchi, "A stable tracking control method for a nonholonomic mobile robot," *Proc. IEEE/RSJ Int. Workshop on Intelligent Robots and Systems*, vol. 3, pp. 1236-41, 1991.

[19] A. Kemurdjian, V. Gromov, et al, "Small Marsokhod configuration," *Proc. IEEE Int. Conf. on Robotics and Automation*, vol. 1, pp. 165-68, 1992.

[20] P. R. Klarer, "Recent developments in the robotics all terrain lunar explorer rover (RATLER) program," ASCE Specialty Conference on Robotics for Challenging Environments, Albuquerque, NM, 1994.

[21] I. Kolmanovsky and N. H. McClamroch, "Application of integrator backstepping to nonholonomic control problems," *Proc IFAC Nonlinear Control Syst. Des. Symp.*, pp. 747-752, 1995

[22] I. Kolmanovsky and N. H. McClamroch, "Developments in nonholonomic control problems," *IEEE Control Systems Magazine*, vol. 15, no. 6, pp. 20-36, 1995.

[23] E. P. Krotkov, R. G. Simmons and W. L. Whittaker, "Ambler: Performance of A Six-legged Planetary Rover," *Acta Astronautica,* vol. 35, no. 1, 1995.

[24] T. McGeer, "Passive dynamic walking," *Int. Journal of Robotics Research,* vol. 9, no. 2, 1989.

[25] R. M. Murray, Z. Li and S. S. Sastry, *A mathematical introduction to robotic manipulation,* CRC Press, 1994.

[26] R. Nakajima, T. Tsubouchi, S. Yuta and E. Koyanagi, "A development of a new mechanism of an autonomous unicycle," *Proc. IEEE/RSJ Int. Conf. on Intelligent Robots and Systems,* vol. 4, pp. 3658-63, 1997.

[27] G. C. Nandy and Y. Xu, "Dynamic model of a gyroscopic wheel," *Proc. IEEE Int. Conf. on Robotics and Automation,* vol. 3, pp. 2683-88, 1998.

[28] G. Oriolo and Y. Nakamura, "Control of mechanical system with second order nonholonomic constraints: Underactuated manipulators," *Proc. IEEE Conf. on Decision and Control,* vol. 3, pp. 1682-87, 1996.

[29] E. Papadopoulos and S. Dubowsky, "Failure recovery control for space robotic systems," *Proc ACC,* vol. 2, pp. 1485-90, 1991.

[30] C. Rui and N. H. McClamroch, "Stabilization and asymptotic path tracking of a rolling disk,", *Proc IEEE Int. Conf. on Decision and Control,* vol 4, pp. 4294-4299, 1995.

[31] F. Saito, T. Fukuda, and F. Arai, "Swing and locomotion control for two-link brachiation robot," *IEEE Control Systems Magazine,* vol. 14, no. 1, pp. 5-12, Feb., 1994.

[32] M. Sampei, T. Tamura, T. Kobayashi, and N. Shibui, "Arbitrary path tracking control of articalated vehicles using nonlinear control theory," *IEEE Trans. on Control System Technology,* vol. 3, no. 1, pp. 125-131, 1995.

[33] C. Samson, "Time-varying feedback stabilization of car like wheeled mobile robot," *Int. Journal of Robotics Research,* vol. 12, no. 1, pp. 55-64, 1993.

[34] N. Sarkar, X. Yun, and V. Kumar, "Control of mechanical systems with rolling constraints: Application to dynamic control of mobile robots," *Int. Journal of Robotics Research*, vol. 13, no. 1, pp. 55-69, 1994.

[35] S. Schael, and C. G. Atkeson, "Robot juggling: implementation of memory-based learning," *IEEE Control Systems Magazine*, vol. 14, no. 1, pp. 57-71, Feb., 1994.

[36] A. Schoonwinkel, "Design and test of a computer stabilized unicycle," Ph.D. dissertation, Stanford Univ., 1987.

[37] Z. Sheng and K. Yamafuji, "Postural stability of a human riding a unicycle and its emulation by a robot," *IEEE Trans. on robotics and automation*, vol. 13, no. 5, pp. 709-20, 1997.

[38] S. J. Singh and D. H. Shin, "Position based path tracking for wheeled mobile robots," *Proc. IEEE/RSJ workshop on the Intelligent Robots and Systems*, vol. 1, pp. 386-91, 1989.

[39] O. J. Sordalen C. and Canudas de Witt, "Exponential control law for a mobile robot: extension to path following," *Proc. IEEE Int. Conf. on Robotics and Automation*, vol. 3, pp. 2158-63, 1992.

[40] M. W. Spong, "The swingup control problem for the acrobot," *IEEE Control Systems Magazine*, vol. 15, no. 1, pp. 49-55, 1995.

[41] D. W. Vos and A. H. von Flotow, "Dynamics and nonlinear adaptive control of an autonomous unicycle: theory and experiment," *Proc. IEEE Conf. on Decision and Control*, vol. 3, pp. 2670-75, 1989.

[42] K. Waldron, *The adaptive suspension vehicle*, MIT Press, 1989.

[43] Bong Wie, *Space vehicle: Dynamics and Control*, AIAA Education Series, 1998

[44] Y. Xu, K. W. Au, G. C. Nandy and H. B. Ben, "Analysis of actuation and the dynamic balancing for a single wheel robot," *Proc. IEEE/RSJ Int. Conf. on Intelligent Robots and Systems*, vol. 4, pp. 3658-63, 1998.

[45] Y. Xu and H. Y. Shum, "Dynamic control and coupling of a free-flying space robot system," *Journal of Robotic Sytems*, vol. 11, no. 7, pp. 573-89, 1994.